Invited review article

Geological and geochemical evolution of the Trincheira Complex, a Mesoproterozoic ophiolite in the southwestern Amazon craton, Brazil

Gilmar José Rizzotto [a,*], Léo Afraneo Hartmann [b]

[a] Geological Survey of Brazil (CPRM), Rua 148, no. 485; 74170-110 Goiânia, Goiás, Brazil
[b] Instituto de Geociências, Universidade Federal do Rio Grande do Sul, Avenida Bento Gonçalves, 9500; 91501-970 Porto Alegre, Rio Grande do Sul, Brazil

ARTICLE INFO

ABSTRACT

We document the first-known Mesoproterozoic ophiolite from the southwestern part of the Amazon craton, corresponding to the Trincheira Complex of Calymmian age, and propose a tectonic model that explains many previously enigmatic features of the Precambrian history of this key craton, and discuss its role in the reconstruction of the Columbia supercontinent. The complex comprises extrusive rocks (fine-grained amphibolites derived from massive and pillowed basalts), mafic–ultramafic intrusive rocks, chert, banded iron formation (BIFs), pelites, psammitic and a smaller proportion of calc-silicate rocks. This sequence was deformed, metasomatized and metamorphosed during the development of the Alto Guaporé Belt, a Mesoproterozoic accretionary orogen. The rocks were deformed by a single tectonic event, which included isoclinal folding and metamorphism of the granulite–amphibolite facies. Layered magmatic structures were preserved in areas of low strain, including amygdaloidal and cumulate structures. Metamorphism was pervasive and reached temperatures of 780–853 °C in mafic granulites and 680–720 °C in amphibolites under an overall pressure of 6.8 kbar.

The geochemical composition of the extrusive and intrusive rocks indicates that all noncumulus mafic–ultramafic rocks are tholeiitic basalts. The mafic–ultramafic rocks display moderate to strong fractionation of light rare earth elements (LREE), near-flat heavy rare earth element (HREE) patterns and moderate to strong negative high field strength element (HFSE) anomalies (especially Nb), a geochemical signature typical of subduction zones. The lowest units of mafic granulites and porphyroblastic amphibolites in the Trincheira ophiolite are similar to the modern mid-ocean ridge basalt (MORB), although they locally display small Ta, Ti and Nb negative anomalies, indicating a small subduction influence. This behavior changes to an island arc tholeiite (IAT) signature in the upper units of fine-grained amphibolites and amphibole rich-amphibolites, characterized by progressive depletion in the incompatible elements and more pronounced negative Ta and Nb anomalies, as well as common Ti and Zr negative anomalies. Tectono-magmatic variation diagrams and chondrite-normalized REE and primitive mantle normalized patterns suggest a back-arc to intra-oceanic island arc tectonic regime for the eruption of these rocks. Therefore, the Trincheira ophiolite appears to have originated in an intraoceanic supra-subduction setting composed of an arc-back-arc system. Accordingly, the Trincheira Complex is a record of oceanic crust relics obducted during the collision of the Amazon craton and the Paraguá block during the Middle Mesoproterozoic. Thus, the recognition of the Trincheira ophiolite and suture significantly changes views on the evolution of the southern margin of the Amazon craton, and how it can influence the global tectonics and the reconstruction of the continents.

© 2012 Elsevier B.V. All rights reserved.

Contents

* Corresponding author. Tel.: +55 62 99725559; fax: +55 62 32401417.
  E-mail address: grgilmarjose@gmail.com (G.J. Rizzotto).

1. Introduction

The paleogeographic continental reconstructions of the Mesoproterozoic commonly propose a link between eastern Laurentia and the western margin of the Amazon craton (Cawood et al., 2007; Dalziel, 1991; Hoffman, 1991; Keppie et al., 2001; Santos et al., 2008; Tohver et al., 2004a,b; Weil et al., 1998). The link between Amazonia and Laurentia is a key issue for the reconstruction of the Mesoproterozoic paleogeography. Over the past decade, different scenarios have been proposed for the evolution of the SW margin of the Amazon craton, primarily based on geochronological data (Bettencourt et al., 2010; Boger et al., 2005; Cordani and Teixeira, 2007; D'Agrella-Filho et al., 2008; Litherland et al., 1989; Sadowski and Bettencourt, 1996; Santos et al., 2000, 2008; Teixeira and Tassinari, 1984; Tohver et al., 2002, 2004a,b). All these previous investigations were conducted on a regional scale, without detailed field information or petrological, geochemical and structural data, limiting their interpretation of tectonic environments involved in the crustal growth of the southwestern Amazon craton. Several tectonic environments have been suggested and are related to the amalgamation of intra-oceanic magmatic arcs or back-arc and Wilson Cycle processes of ocean opening and closing (accretionary orogens). However, thus far, only Tohver et al. (2004a, 2006) have indicated the location of a suture zone between the adjoining Amazonia and Laurentia. In this work, we provide detailed field information and geochemical data which allow advancements in understanding the tectonic setting of the southwestern margin of the Amazon craton.

Distinguishing between accreted-terrane and terrane boundaries and sutures that separate different cratons or orogens involved in continent–continent collisions may be difficult because the distinction depends on identifying juxtaposed terranes that had significantly different magmatic and lithotectonic histories prior to collision but share a common history afterwards. Accretionary orogens may also be referred to as non-collisional, exterior orogens or zones of type-B subduction formed at intraoceanic and continental margin convergent plate boundaries. They form at sites of subduction of the oceanic lithosphere and include the supra-subduction zone forearc, magmatic arc and back-arc components (ophiolites) (Cawood et al., 2009). A large proportion of juvenile mafic to silicic calc-alkaline igneous rocks are involved, as well as their volcanosedimentary products. Large volumes of rocks from accretionary belts exhibit typical juvenile isotopic signatures, indicating essentially mantle-derived parental magmas. Ophiolites can be part of these environments as remnants of an allochthonous or autochthonous ancient oceanic crust and upper mantle incorporated into an orogenic belt. Thus, ophiolites are of prime importance to an understanding of orogens and are essential to the definition of a suture zone. One of the difficulties in the study of ophiolite complexes in deformed regions is that they are generally emplaced early and undergo considerable deformation and alteration during subsequent orogenic events.

Therefore, the identification of oceanic crust relics in ophiolites along a suture zone at which the Amazon craton collided with the Laurentia or Paraguá block to form a supercontinent has remained enigmatic for many years, despite intense study of the poorly exposed SW portion of the Amazon craton. Tohver et al. (2004a) believe that the E–W trending Nova Brasilândia belt marks the limit between the Amazon and Paraguá cratons and formed during the late Mesoproterozoic. However, the Nova Brasilândia belt has no petrotectonic association compatible with a suture zone and was interpreted as a rift-passive margin (Rizzotto, 1999). To date, there are no known ophiolites in the southwestern margin of the Amazon craton.

Most modern ophiolites have subduction zone chemical characteristics, indicating their magmatic and tectonic association with supra-subduction zone processes (Dilek et al., 1999; Ishikawa et al., 2002; Shervais, 2001; Stern and Bloomer, 1992). The well-studied Tethyan ophiolites show a common geochemical progression in their magmatic evolution from initially MORB-like to IAT to boninites. In general, these ophiolitic complexes show an internal stratigraphy and chemical composition represented by a lower suite of relatively evolved IAT lavas, a middle suite of depleted arc tholeiite rocks, and a stratigraphically higher suite of highly depleted boninitic rocks (Dilek and Furnes, 2009). The evolution in the geochemical behavior of magma from MORB-type to IAT is characterized by a progressive depletion of the incompatible elements and more pronounced negative Ta and Nb anomalies, as well as negative anomalies of Ti and Zr.

The recognition of ancient tectonic environments based on only their geochemical characteristics is restricted by chemical similarity and alteration. The uncertainty about the tectonic setting where such ophiolites formed is due to the common occurrence of MORB-like lavas, in addition to those more indicative of a suprasubduction zone setting (IAT). Likewise, several examples in the literature show us that the geochemical characteristics of Archean mafic–ultramafic volcanic rocks provide important information for understanding the evolution of the initial mantle–crust system (Arndt et al., 1997; Jochum et al., 1991; Polat et al., 1998; Puchtel et al., 1998; Sun, 1987). Similarly, the geochemical characteristics of modern volcanic rocks of different tectonic environment are distinct in terms of the behavior of HFSE, LFSE and REE (Pearce and Cann, 1973; Sun and McDonough, 1989).

In the case of the oceanic crust, studies of modern island arc basalts suggest that subduction of the oceanic lithosphere, with or without associated sediment, can continuously modify the chemical, isotopic and mineralogical composition of the overlying mantle wedge. The release of fluids and hydrous silicate melts from the down-going altered oceanic crust can result in the enrichment of incompatible elements in the mantle wedge above the subduction zone. In this context, back-arc basin basalts are MORB-like, with a subtle subducted slab flux component made evident by elevated large ion lithophile element (LILE) abundances. These abundances exhibit the typical spiked pattern of subduction-related arc basalts on multi-element plots, but the pattern is more subdued than that of arc basalts (Hawkins et al., 1994; Jenner et al., 1987). More recently, this geochemical duality (MORB to IAT) has been ascribed to the progressive depletion and metasomatism of a common melt source over the course of ophiolite formation (Dilek and Furnes, 2009). In other words, all magmatic components (i.e., MORB, IAT, and boninite) may have formed in the same oceanic environment, which witnessed the eruption of MORB-like lavas followed by IAT and boninites.

Our proposal of the existence of an ancient ocean crust in the southwestern Amazon craton represented by the Trincheira Complex is supported by field data, mineral chemistry and whole-rock geochemistry (mainly REE and trace elements). Thus, we follow the original methodology that established the ophiolite concept, based largely on field, petrological, and geochemical studies.

In this study, we present field data, mineral chemistry and whole-rock geochemistry to test this hypothesis. We emphasize trace elements and REE content to characterize the geotectonic environment and the evolution of magmatism that generated the Trincheira Complex. The result of this study is the recognition of ophiolites and their dismembered fragments and the concurrent identification of chemically distinct island-arc/back-arc volcanic and plutonic complexes. Preserved oceanic lithosphere commonly occurs along major tectonic sutures. The presence of oceanic lithosphere in the Alto Guaporé Belt and the evaluation of its origin establish constraints for tectonic reconstructions of the southwestern Amazon craton and provide some key issues related to reconstruction of the pre-Rodinia supercontinent.

2. Geological framework and field characteristics

The studied area is located on the boundary between the Sunsás and Rondônia–Juruena Provinces (Santos et al., 2008), southwestern Amazon craton (Fig. 1). Rizzotto et al. (2002) used geological and geochronological data to characterize a regional tectono-magmatic event with ages in the range of 1350 to 1320 Ma. Rizzotto and Dehler (2007) later called the resulting orogen the Alto Guaporé Mobile Belt (AGB) and interpreted it as having been derived from an accretional–collisional orogeny under conditions of medium to high metamorphic grade. The belt has the same temporal delimitation as the San Ignacio Orogeny in eastern Bolivia (Litherland et al., 1986) and the Rondonian (Teixeira and Tassinari, 1984) and Candeias (Santos et al., 2002) orogenies. This study reports new data that indicate that the Alto Guaporé Belt contains juvenile magmatism aged 1468–1447 Ma that was reworked at 1350–1320 Ma (Rizzotto et al. unpublished data).

The Alto Guaporé Belt (WNW–ESE trend) is a large geotectonic feature extending from the southeastern portion of Rondônia to the southwestern portion of Mato Grosso, integrating an area of 1900 km^2, 95 km long by 20 km wide. The southern part of the complex is covered by the Cenozoic sediments of the Guaporé basin. Interpretation of the aeromagnetic data suggests a continuity of the Alto Guaporé Belt to the west–northwest along at least 400 km below the Phanerozoic cover, but geological observations suggest that it may extend up to 1000 km, reaching the Andean Cordillera. Its northern boundaries are the Nova Brasilândia Terrane, Uopianes Basin, and Rondônia–Juruena Province.

To the south, the boundaries are hidden below the Phanerozoic sedimentary rocks of the Guaporé basin (Fig. 2).

The Alto Guaporé Belt is primarily represented by the Trincheira Complex of mafic–ultramafic rocks initially described by Romanini (2000) and the Rio Galera Complex of dioritic–tonalitic rocks, in addition to various bodies of mafic–felsic intrusives (granitoids and gabbros) (Fig. 3). Typically of the oceanic domain the Trincheira Complex is composed of several disrupted, highly dismembered imbricate thrust slices forming an incomplete ophiolite sequence (Fig. 4).

The disrupted complex has an apparent stratigraphic sequence of layered mafic–ultramafic cumulates, intrusive mafic–ultramafic and extrusive mafic rocks with interbedded sedimentary clastic and chemical sequences. The deformation is heterogeneous, as indicated by highly deformed zones adjacent to areas with poorly developed foliation or a partly preserved primary texture. Although the original stratigraphy is not recovered here because of its structural complexity, superimposed metamorphism and sparsity of outcrops, the complex is divided into three units: a) Lower Unit: layered mafic–ultramafic (granulite-facies metamorphism): mafic granulites that has as protolith olivine orthopyroxenite, bronzitite, and websterite; b) Intermediate Unit: intrusive mafic (amphibolite-facies metamorphism): banded amphibolites which has as protolith norite, gabbronorite, gabbro, anorthosite, gabbroanorthosite and rare plagiogranite; and c) Upper Unit: extrusive mafic rocks (amphibolite-facies metamorphism): fine-grained amphibolites (massive and pillowed basalt) with intercalations of chemical and sedimentary sequences consisting of metachert (BIFs), calc-silicate rocks and aluminous schist/quartzite. The close spatial relationship between the mafic intrusives of the intermediate unit and the extrusive rocks with comparable deformation and metamorphism suggests that they are cogenetic. Granulite-facies metamorphism ranges from the basal portions of the complex to amphibolite-facies in the upper zone of the complex with retrogression to middle amphibolite facies in an anastomosing network of mylonitic shear zones (Fig. 5a).

Mafic–ultramafic cumulates of the lower unit in the southern part of the complex have mostly anhydrous granulite-facies parageneses of olivine–orthopyroxenite, bronzitite and websterite protoliths. These are interlayered with rare plagiogranites and show transposed igneous banding into vertical structures. Narrow mylonitic shear bands cut granulitic rocks and turn them into amphibolites or tremolitites, actinolitites, serpentinites and actinolite-talc schists in variable proportions, derived from the deformation of the ultramafic components. Locally, these cumulate rocks are intruded by coarse-grained granitic dikes and dioritic–tonalitic rocks. The textures of the mafic–ultramafic granulites (Vernon, 1970) are fine-grained granoblastic aggregates with polygonal grain boundaries and common triple junctions. The characteristic mineral assemblage of metamorphosed mafic rocks is orthopyroxene + clinopyroxene ± plagioclase ± olivine throughout the entire granulite zone, with minor Ti-biotite, brown hornblende and ilmenite.

Norite, gabbronorite, gabbro, anorthosite and gabbroanorthosite intercalated in the lower sequence display cumulate textures commonly cut by high-angle, mm- to cm-scale mylonitic shear zones that have diffuse to sharp boundaries with the surrounding, slightly deformed or undeformed gabbros. These are usually present as layered bodies with primary compositional banding transposed into vertical structures by tectonic superposition and transformed into banded amphibolites. Additional observations include millimeter- to centimeter-thick alternate felsic layers composed of plagioclase and rare amphibole and mafic bands of amphibole cumulates (originally pyroxene), and intermediate layers rich in plagioclase + amphibole + ilmenite ± titanite ± epidote ± quartz (Fig. 5b).

Amphibolites become predominant upward in the plutonic sequence, where multiple and mutually intrusive relations between granoblastic amphibolites (deformed small bodies of pyroxenites) and leucocratic metagabbros are common. The mylonitic foliation has a high dip (>60°) to the SSW and a mineral lineation down-dip (>50°).
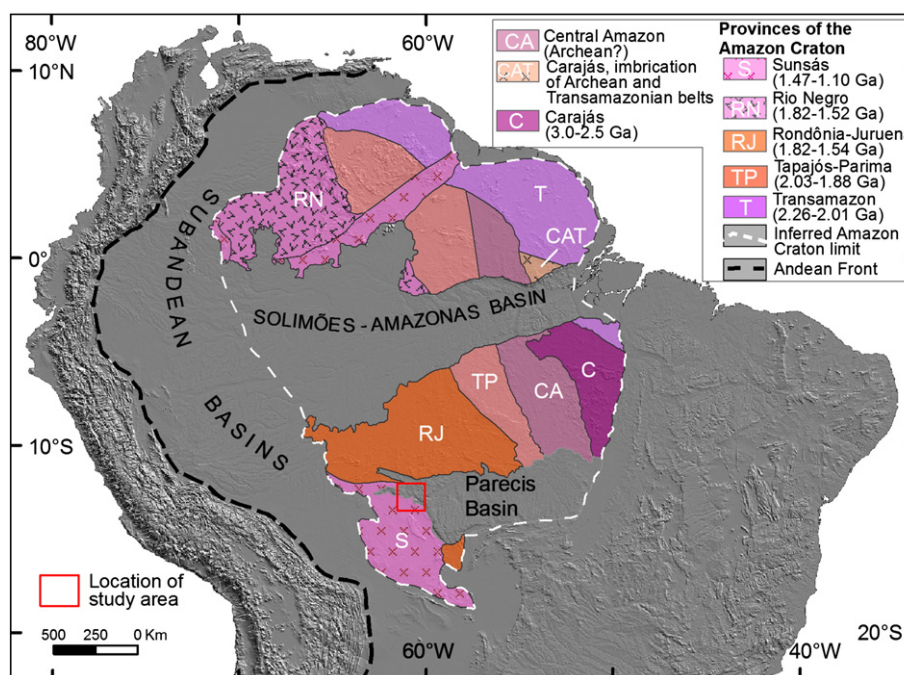
Fig. 1. Major geochronological provinces of the Amazon craton and main Phanerozoic basins. Modified from Santos et al. (2008).

Metamorphic banding and closed-isoclinal and asymmetric folds are generally associated with tectonic foliation (Fig. 5c). The adjacent amphibolites and metasedimentary rocks are structurally conformable.

The amphibolites occur in the southeastern sector of the mafic–ultramafic complex. They are usually mylonitic, banded and folded, and fine-grained; rarely isotropic; commonly tectonically interlayered with dioritic–tonalitic gneiss, banded metagabbro, metagabbronorites, leucometagabbros and metapyroxenites. The units show a strong to vertical tectonic transposition. In zones of high strain, the amphibolites are fine-grained, with regular and uniform banding in the centimeter–millimeter scale displayed as a heterogeneous segregation of felsic bands of plagioclase and quartz alternating with mafic bands composed of amphibole. These lenses of amphibolites occur in sub-vertical positions as a result of compressive deformation. Isoclinal folds are frequent, as well as thin quartz veinlets that define ptigmatic and intrafolial folds. In some locations, isoclinal folding and thickening of the hinge zone can be observed (Fig. 5c). In a few places, centimetric to metric pegmatoidal veins composed of K-feldspar, quartz and amphibole are observed, which were likely generated by the late segregation of hydrothermal fluids.

The upper unit is distributed in the northwestern sector and represented predominantly by fine-grained, gray amphibolites, which locally present partially preserved igneous textures and structures and can be characterized as metabasalts. These show a pervasive sub-horizontal jointing with centimeter spacing, representing subaerial volcanism (Fig. 5d). Millimeter- to centimeter-sized cavities are filled with an aggregate of epidote, garnet and quartz and may correspond to deformed amygdules (Fig. 5e) in relict pillow lavas. Likewise, bands of fine-grained, white material composed of quartz + plagioclase + epidote ± carbonate ± sulfide (interpillow material) bordering the better-preserved cores of the metabasalts resemble pillow structures (Fig. 5f). However, the high strain makes this identification questionable. Restricted bands with high sulfidation are common in fine-grained amphibolites affected by late, low-grade metamorphism (retrometamorphism), which transformed the rock into an assembly composed of actinolite + epidote + albite + quartz + pyrite ± chalcopyrite.

Pods of mafic–ultramafic rocks occur as bodies of several tens of meters contained in fine-grained amphibolites and suggesting intrusions in the form of sills. They occur as subrounded to elongated blocks with preserved cores and sheared edges, usually distributed along the direction of the regional metamorphic foliation. They are mostly massive, coarse-grained, have a dark green to black color and outcrop as metric subangular boulders and a few bodies that are hundreds of meters in length (Fig. 6a). The pods occur along the zones with least deformation where the flow of metamorphic fluids is concentrated in low-pressure areas, often in the hinges of folds in pyroxenite and melagabbro protoliths. They often exhibit granoblastic aggregates of amphibole as well as porphyroblasts (up to 8 cm) surrounded by irregularly shaped grains of plagioclase (Fig. 6b). They are classified as porphyroblastic amphibolite with partially preserved igneous texture and structure. Nevertheless, they show a heterogeneous pattern in the behavior of the flow direction of metamorphism, with variation in the foliation trend depending on the rheology of the rock (Fig. 6c). Therefore, some outcrops contain megapods surrounded by shear bands in which the original rock has been partly transformed into ultramafic schist (actinolite schist, talc schist, and tremolitite) (Fig. 6d). Metamorphic foliation rarely develops in the central parts of larger bodies, indicating a greater strength in relation to the same strain.

The fine-grained amphibolites are overlain by supracrustal rocks consisting of metacherts, calc-silicate rocks, banded iron formations (Fig. 7a), mylonitic gneiss, pelitic schists and aluminous quartzite. The clastic and chemical supracrustal rocks occur as lenses with elongated and sigmoidal forms and dimensions ranging from a few meters to kilometers in length. They are composed of biotite–muscovite–quartz schist, garnet–sillimanite–biotite schist, sillimanite–staurolite–biotite–quartz schist, sillimanite–garnet gneiss (Fig. 7b), hematite–magnetite quartzite, metamarls, and scarce kyanite quartzite. Generally, schists show pervasive ptigmatic folds constituted primarily of quartz and feldspar and lenses of quartz boudin, which are often generated by metamorphic segregation (Fig. 7c). Polycrystalline aggregates of quartz form less altered cores which were preserved from deformation along the sigmoidal foliation (Fig. 7d). Associated with the schists is a striking presence of metric veins (more rarely decametric) of white quartz with
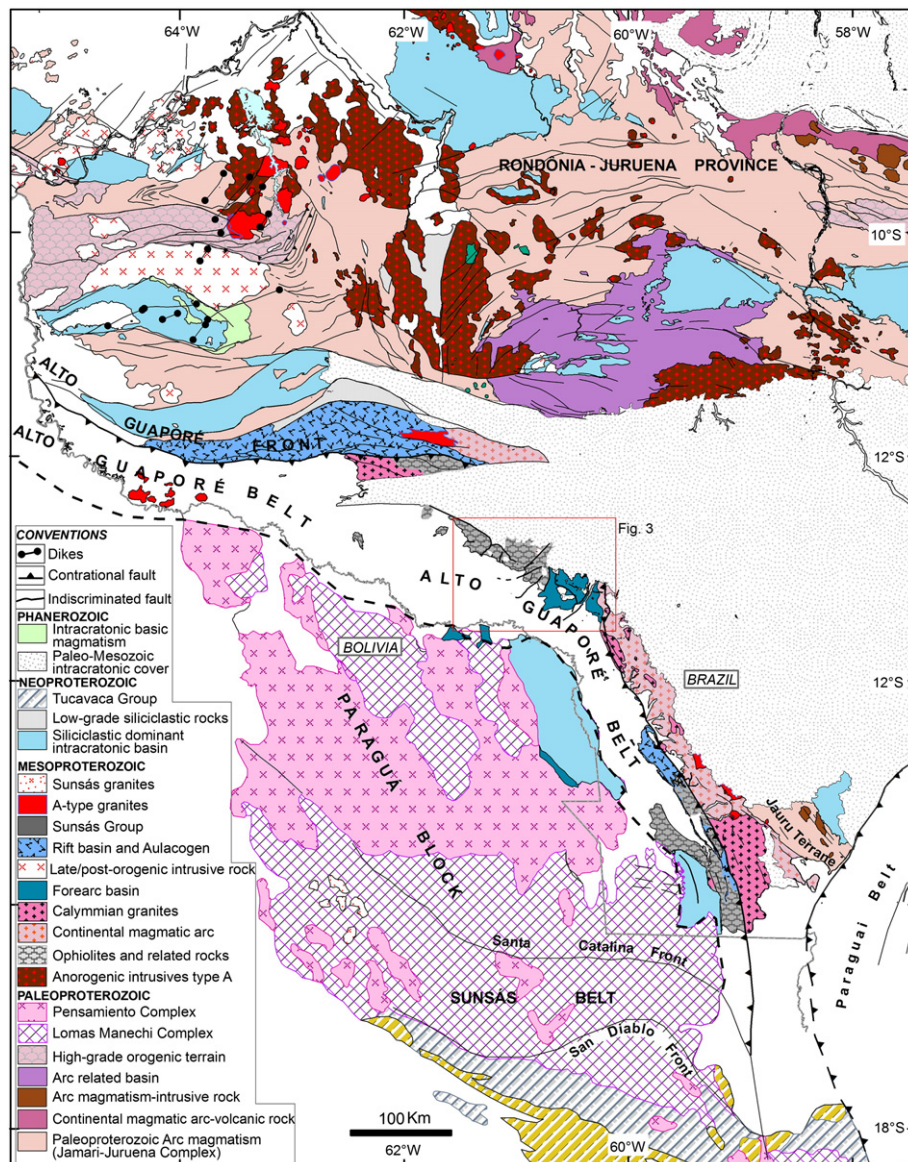
Fig. 2. Simplified map of the southwestern Amazon craton showing the approximate boundaries of the main terranes and belts, tectonic elements, and lithologic units. Modified after Rizzotto (2010) and Schobbenhaus (2001).

sporadic centimeter muscovite plates, which form small ridges aligned along the regional foliation.

Farther to the southeast, two more bodies of ultramafic rocks may be part of the ophiolitic sequence; they are referred to as Morro sem Boné and Morro do Leme. They consist of strongly serpentinized ultramafic rocks that are exposed discontinuously as two bodies layered within the metavolcanic–sedimentary sequence. The Morro sem Boné is a unique body elongated in a NE–SW trend and is approximately 5.5 km long and 1.0 km wide. It is intrusive into pelitic–psamitic supracrustal rocks. Its upper portion is predominantly composed of serpentinites, which exhibit strong sub-horizontal fracturing and intercalations of laterite and siliceous silcrete layers. The serpentinite grades at a lower topography into dunite, which is strongly fractured and transformed into a network of aggregates of serpentine, magnesite, silica and microcrystalline garnierite. Lenses of pyroxenite are intercalated with the dunite. Narrow lenses of amphibolites and actinolite schist were generated by shearing the pyroxenites.

In general, the rocks have a brittle–ductile foliation of an approximately N20E direction, subconcordant with the general direction of

the massif. In the serpentinite, the original rock has been completely transformed because iron–magnesium minerals were leached and replaced by microcrystalline silica and iron oxides. In some places, the rock is porous and has low density, depending on its degree of alteration. A mesh-like texture was formed by the aggregate of fibrous serpentine surrounding the olivine. In drill cores, granite intrusions were observed in the layered dunites.

3. Petrography and mineral chemistry

The mineralogical characteristics and interpreted protoliths of the different types of mafic–ultramafic rocks are presented in Table 1. These rocks show metamorphic assemblages with penetrative foliation. The primary igneous mineralogy and texture are preserved in some rocks. Based on the mineral assemblages of the metamorphosed mafic–ultramafic rocks, two metamorphic zones are distinguished: a granulite zone (orthopyroxene + clinopyroxene + plagioclase ± olivine) and a large amphibolite zone (hornblende + plagioclase ± clinopyroxene + ilmenite + titanite ± epidote) resultant from retrogressive metamorphism of the granulite by continuous deformation during uplift and
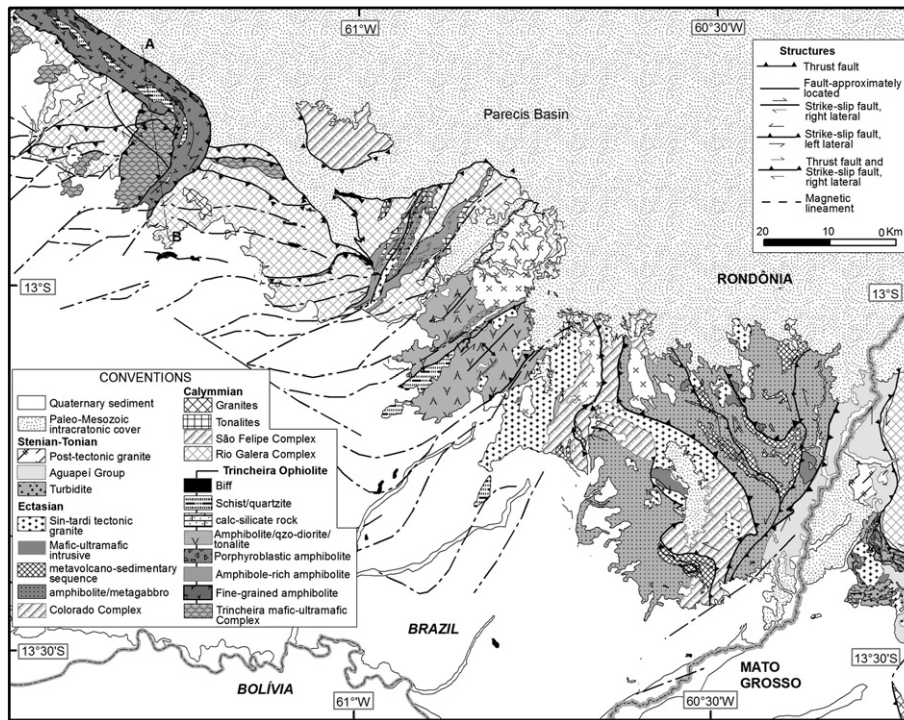
Fig. 3. Simplified geological map of our study area in southeastern region of Rondônia and southwestern of Mato Grosso, Brazil. A–B depicts the profile line for the structural cross-section shown in Fig. 4.

exhumation. Igneous and metamorphic minerals are not easily distinguished on textural grounds in granulite-facies metamorphic rocks in the region.

Mafic granulites have relict igneous textures consisting of elongated and curved, wedge-shaped and plane twinning crystals (<2 mm) of plagioclase. The crystals are surrounded by a granoblastic, polygonal and isogranular matrix (<1 mm) consisting of plagioclase, diopside and orthopyroxene. Relict igneous porphyroclasts (orthopyroxene + plagioclase) (Fig. 8a) are usually deformed, elongate crystals partially replaced by metamorphic minerals. In contrast with the metamorphic pyroxene, the igneous pyroxene has ubiquitous exsolution lamellae, while metamorphic orthopyroxene recrystallizes in granoblastic polygonal aggregates. The contacts are polygonal, with angles of 120°. The orthopyroxene is partially transformed along the rims into tschermakitic hornblende. In shear micro-zones, magnesio-hornblende forms intergrowths with cummingtonite, carbonate and rare quartz.

Magnesio-hornblende in fine-grained amphibolites occurs as prismatic aggregates; together with epidote, they define the penetrative foliation of the rock. Amygdules elongated by deformation are filled with prismatic crystals of epidote and a fine granoblastic aggregate of quartz + albite + ilmenite ± sulfides (Fig. 8b). The preserved igneous features are represented in amygdaloidal zones (Fig. 8c), suggesting a basaltic protolith (pillowed basalt).

Amphibole-rich amphibolites are spatially associated with fine-grained amphibolites. The mineral assemblage is shown in Table 1 and Fig. 8d. Prismatic crystals and acicular actinolite surround the porphyroclasts of magnesio-hornblende in some areas. The presence

of ghost crystals as porphyroclasts of pyroxene partially replaced by magnesio-hornblende is also common. The sigmoidal penetrative foliation is defined by the elongated prisms of amphibole and rare chlorite (Fig. 8e). Relict igneous texture (ophitic texture) is observed locally and granoblastic aggregates of plagioclase + quartz occur between the interstitial spaces of the amphibole.

Porphyroblastic amphibolites are less abundant than amphibole rich-amphibolites. The porphyroblastic aggregates of magnesio-hornblende with subrounded to elongated inclusions and fillets of quartz along the planes of cleavage suggest the replacement of igneous pyroxene by amphibole (Fig. 8f). Plagioclase and quartz aggregates in a mosaic of 120° occur between amphibole porphyroblasts.

Metaultramafic rocks are represented by orthopyroxene cumulates (Fig. 8g), which exhibit an adcumulate texture represented by their imbrication in a triple junction at angles of 120° of large crystals of orthopyroxene. Rare post-cumulus crystals of plagioclase, magnetite and cummingtonite make up approximately 1%.

The metagabbros are coarse-grained and have the best-preserved primary igneous features among the rocks (Fig. 8h). Metagabbro bodies often escape pervasive internal deformation and this, in turn, prevents the access of water, hampers recrystallization and hinders hydratation of the igneous minerals. Ophitic and intergranular textures are present. However, plagioclase simplectites + hornblende develop at the edges of the pyroxene. Throughout shear microzones the primary minerals (plagioclase) are transformed to albite + epidote + quartz and the pyroxene is partially transformed into amphibole. The metamorphic changes are most evident at the edges
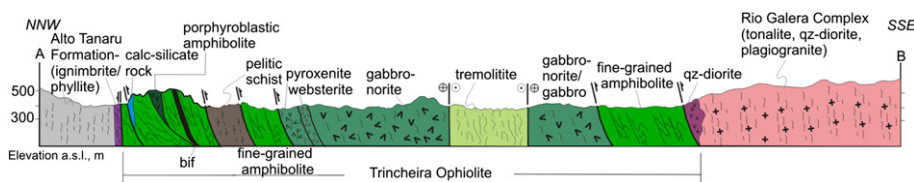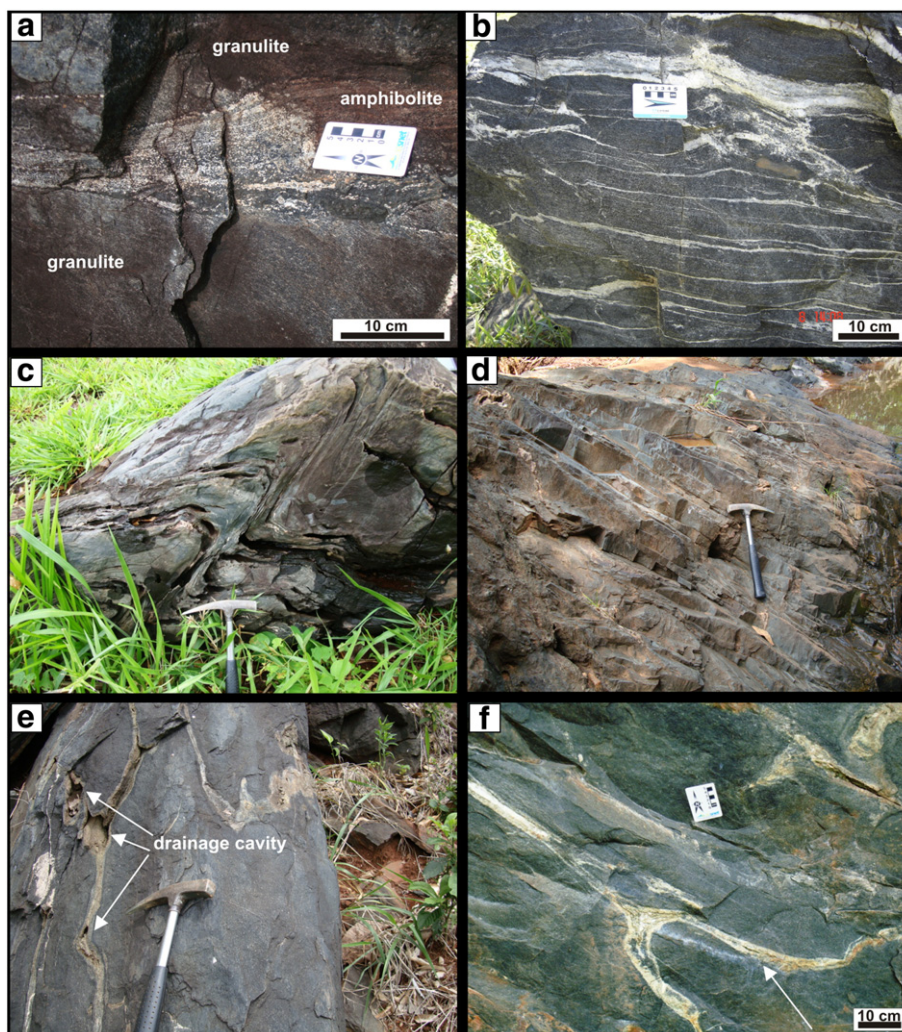

Fig. 4. Structural cross-sections (A–B) across the Trincheira ophiolite.

Fig. 5. Mafic and ultramafic rocks of the Trincheira Complex. (a) Mafic granulite cross-cutting for amphibolite shear band; (b) banded amphibolite; (c) tight fold in amphibolite into zone of high strain; (d) subhorizontal jointing in amphibole rich-amphibolite; (e) drainage cavities in fine-grained amphibolite; (f)) structures similar to stretched pillow lavas. On the arrow, interpillow material.

of the clinopyroxenes, where there is simplectitic intergrowth of magnesio-hornblende + plagioclase. Crystals of orthopyroxene are pseudometamorphosed to cummingtonite and magnesio-hornblende.

3.1. Analytical methods

Mineral analyses of mafic–ultramafic rocks were performed on polished thin sections of orthopyroxene, clinopyroxene, amphibole and plagioclase using a JEOL JXA-8530F EPMA five-spectrometer electron microprobe at the University of Western Australia. Online Table 1 presents representative compositions of these minerals. The analytical conditions were an accelerating voltage of 15 kV and a beam current of 20 nA. The elements analyzed and their standards were as follows: Na (jadeite), Mg (periclase), Al (corundum), Si (wollastonite), K (orthoclase), Ca (wollastonite), Ti (rutile), Cr (Cr metal), Mn (Mn metal) and Fe (Fe metal). All analytical X-ray lines were K alpha; counting times were 20 s for both peaks and backgrounds.

3.2. Results

3.2.1. Amphibole

The mafic granulites contain brown and greenish-brown amphiboles. According to Leake's (1978) classification, brown amphibole is ferro-tschermakitic hornblende and greenish-brown amphibole is

tschermakite (Fig. 9a), with magnesium number (Mg#) between 0.47 and 0.72 and high TiO_2 and Al_2O_3 contents. Their Al^{iv}/Al^{vi} ratios are <3.3, suggesting a secondary (metamorphic) origin. Although amphibole crystals are generally unzoned, they rarely show a lamellar intergrowth between tschermakite and cummingtonite. Green amphibole (magnesio-hornblende) occurs in close microshear zones that cut granoblastic mafic granulites. These amphiboles are similar to those of the adjacent amphibolites. The porphyroblastic amphibolite, fine-grained amphibolites and amphibole rich-amphibolite contain greenish-brown and green amphiboles, which vary from tschermakitic hornblende to magnesio-hornblende (Fig. 9a). Its Mg# value varies between 0.46 and 0.60, with TiO_2 and Al_2O_3 contents between 0.22 and 0.91 wt.% and between 5.5 and 16.4 wt.%, respectively.

3.2.2. Orthopyroxene

Metamorphic orthopyroxene and Ca-clinopyroxene coexist in the mafic granulites of the Trincheira Complex. To distinguish between the igneous orthopyroxene and metamorphic orthopyroxene, we utilized a graphic that uses the ratio $Fe_{total} + MgO$ versus Al_2O_3 (Bhattacharyya, 1971) (Fig. 9b), which is from unambiguously metamorphic orthopyroxene.

Orthopyroxene in mafic granulites has an enstatite to ferrosillite composition (Fig. 9c). The compositions of pyroxene are listed in
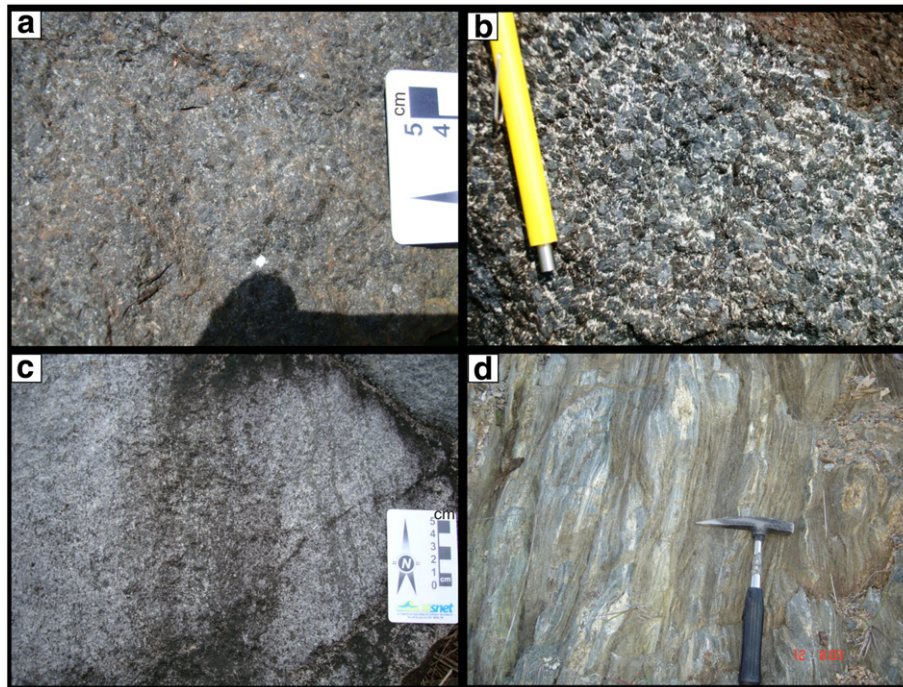
Fig. 6. Rocks of the Trincheira Complex. (a) massive, coarse-grained, ultramafic rock; (b) granoblastic texture of the porphyroblastic amphibolite; (c) metamorphic microbanded in metapyroxenite; (d) shear bands, where the original rock has been partly transformed for ultramafic schist.

the Online Table 1. The Mg# ranges between 0.48 and 0.61, with Cr_2O_3 and TiO_2 contents varying between 0 and 0.03 and 0 and 0.08 wt.%, respectively. Al_2O_3 decreases from the core (1.92 wt.%) to the overgrowth rim (1.08 wt.%).

3.2.3. Clinopyroxene

Clinopyroxene in the mafic granulites (En_{25-35}, Wo_{45-47}, Fs_{18-30}) is diopside; in one analysis, it is hedenbergite (Fig. 9d). It has an

Mg# between 0.85 and 1.90 and Cr_2O_3 and NiO contents between 0 and 0.09 wt.% and 0 and 0.019 wt.%, respectively. Al_2O_3 and TiO_2 contents range from 0.62 to 2.35 wt.% and 0.01 to 0.26 wt.%, respectively (Online Table 1).

3.2.4. Plagioclase

Plagioclase in both mafic granulites and amphibolites is almost unzoned. Although twinning is completely destroyed in most cases,
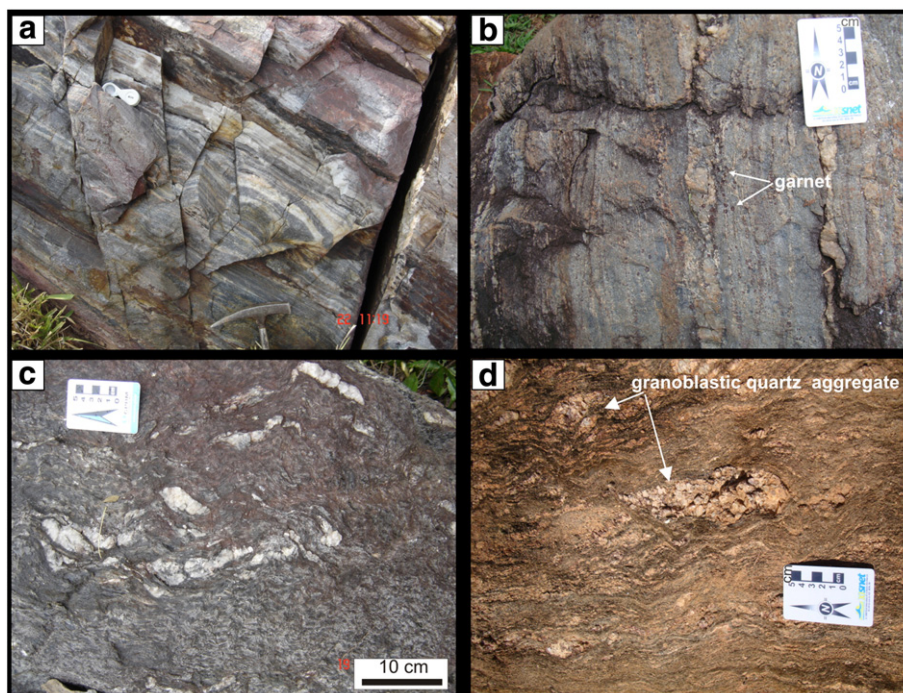
Fig. 7. Field pictures of various types of supracrustal rocks of the Trincheira ophiolite. (a) Alternating layers of chert and magnetite (BIFs) in transpressional zone; (b) aluminous banded gneiss; (c) lenses of the quartz boundin in pelitic schist; (d) biotite–quartz schist with quartz polycrystalline aggregates preserved in sigmoidal shape.

Table 1
Characteristics mineralogical and protolith interpreted of the main rock types Trincheira Complex.

Lithology	Mineralogical composition	Protolith
Mafic granulite	Plagioclase (40–50%) + orthopyroxene (20–25%) + diopside (15–20%) + tschermakitic hornblende (3–5%) + ilmenite (<1%) ± olivine ± cummingtonite	Gabbronorite, norite
Fine-grained amphibolite	Tschermakite or magnesio-hornblende (60–65%) + plagioclase (15–20%) + quartz (5–10%) + epidote (7–10%) ± magnetite ± titanite ± garnet	Basalt
Amphibole-rich amphibolite	Magnesio-hornblende or tschermakite (65%) + plagioclase (20%) + quartz (9%) + epidote (2%) ± titanite ± ilmenite ± actinolite	Hornblende gabbro/melagabbro
Porphyroblastic amphibolite	Magnesio-hornblende (70–80%) + plagioclase (15–20%) + quartz (3–6%) + magnetite (1–2%) ± augite ± ilmenite ± apatite ± epidote	Gabbronorite
Metaultramafic rock	Orthopyroxene (90–95%) + clinopyroxene (5–10%) ± cummingtonite ± plagioclase ± olivine	Pyroxenite, websterite
Metagabbro	Plagioclase (50–60%) + clinopyroxene (25–30%) + orthopyroxene (10–15%) + tschermakite or magnesio-hornblende (5%) ± ilmenite ± titanite ± scapolite	Gabbro

it is still discernible in some crystals. In the mafic granulites, the plagioclase is labradorite (An$_{61-67}$). In one sample, the plagioclase is bytownite (An$_{75}$), while in the amphibolites it varies from andesine to labradorite (An$_{36-65}$) (Fig. 9e). In amphibole rich-amphibolites, the plagioclase medium grains in the matrix are zoned, with core compositions of An$_{62}$ decreasing to An$_{36}$ toward the rims. Plagioclase is often transformed to epidote in the amphibole-rich amphibolites and fine-grained amphibolites.

3.3. P–T estimates

The temperatures and pressure during the metamorphism of the Trincheira mafic–ultramafic Complex have been estimated using the hornblende-plagioclase thermometer of Holland and Blundy (1994) and the aluminum-in-hornblende geobarometry (in the absence of garnet) of Schmidt (1992), respectively. The temperatures were calculated for plagioclase_amphibole pairs that show clear contacts at their boundaries from samples of both granulites and amphibolites. For the specific pressure of 6.8 kbar, temperatures of 820–853 °C and 680–720 °C were estimated for mafic granulites and amphibolites, respectively. Also, we use clinopyroxene–orthopyroxene (two-pyroxene geothermometer) in the mafic granulites to establish a solvus temperature, based on the miscibility gap and the distribution of Ca and Na between both pyroxenes and Fe–Mg exchange reaction between the mineral phases of the geothermometer, according to the empirical calibrations of Wood and Banno (1973). Phase chemistry calculations on granulites show ambient P–T conditions to have been in the range 780–820 °C (clinopyroxene–orthopyroxene equilibria), a temperature value close to those calculated by hornblende-plagioclase thermometer of Holland and Blundy (1994).

The above P–T estimates in both geothermometers are in agreement with an overall metamorphic overprint under granulite (c. 780–853 °C and 6.8 kbar) and amphibolite (c. 680–720 °C and 6.4 kbar) facies conditions. The peak metamorphic conditions (i.e., 850 °C and 6.8 kbar) correspond to a burial depth of c. 20–30 km.

4. Whole-rock chemistry

4.1. Analytical methods

The samples were pulverized using an agate mill at a 150-mesh fraction in the laboratory of Geological Survey of Brazil-CPRM, and the analyses were performed at Acme Analytical Laboratories Ltd. (Vancouver, Canada). The samples were mixed with lithium metaborate and lithium tetraborate and fused at 1000 °C in an induction furnace. The molten beads were rapidly digested in a solution of 5% HNO$_3$ containing an internal standard and mixed continuously until complete dissolution. The loss on ignition (LOI) was determined by measuring the weight lost during heating at 1000 °C over a three-hour period.

Major elements and several minor elements were determined by emission spectrometry (ICP), while the trace elements and REE were determined by mass spectrometry (inductively coupled plasma mass spectrometry—ICP-MS). Additionally, a fraction of 0.5 g was removed for digestion in aqua regia (heated to 95 °C) and analyzed for base metals and precious metals by mass spectrometry (ICP-MS). The accuracy and precision of the geochemical data are presented in the Online Appendix.

Selected elements were normalized to primitive mantle (pm) (Hofmann, 1988) and chondrite (cn) (Sun and McDonough, 1989). Nb (Nb/Nb*), Zr (Zr/Zr*), Ti (Ti/Ti*) and Eu (Eu/Eu*) ratios were calculated with respect to the neighboring immobile elements, following the method developed by Taylor and McLennan (1985). The samples were recalculated to a 100% anhydrous basis for inter-comparisons. Mg numbers (Mg#) were calculated with a molecular ratio of 100 Mg/(Mg + Fe^{2+}), assuming that Fe$_2$O$_3$/FeO = 0.15.

4.2. Results

The data of major elements, trace elements, REE and inter-element ratios of the most significant mafic–ultramafic rocks of Trincheira Complex are presented in Table 2 and Online Table 2. Based on the characteristics of the field, petrographic study and the abundance of major elements (e.g., SiO$_2$ and MgO), the metavolcano-plutonic rocks can be divided into five main groups: (1) fine-grained amphibolite, (2) amphibole rich-amphibolite, (3) porphyroblastic amphibolite, (4) mafic granulite, and (5) mafic–ultramafic cumulate.

Before considering a petrogenetic interpretation, an investigation was conducted to evaluate the geochemical mobility of elements by hydrothermal alteration, amphibolite to granulite facies metamorphism, polyphase deformation and the metasomatism eventually suffered by the mafic–ultramafic rocks of the sequence.

Many petrochemical studies have demonstrated that Zr is one of the least mobile elements in the geochemical system (Pearce and Peate, 1995; Pearce et al., 1992; Winchester and Floyd, 1977). This element has been used as an independent index of geochemical variation for studies of both the geochemical behavior of modern volcanic rocks (Murton et al., 1992) and Archean rocks (Polat et al., 2002). Therefore, we adopted a similar procedure in this study to evaluate the effects of the changes in the mafic–ultramafic rocks.

The mobility of K, Rb, Na, Ba, Sr, Ca, P and Fe has been demonstrated in studies of metamorphosed volcanic rocks (Arndt, 1994; Brunsmann et al., 2000; Frei et al., 2002). In contrast, REE, HFSEs, Al, Cr and Ni have lower mobility (Jochum et al., 1991; Ludden et al., 1982). However, the mobility of the elements of each case must be tested. An effective method was proposed by Cann (1970), in which an immobile element is plotted on the horizontal axis of a diagram of bivariate variation and the element to be evaluated is plotted on its vertical axis. This was used as a criterion to evaluate the effects of alteration and the magnitude of correlation of Zr in binary diagrams (Fig. 10). Elements with a
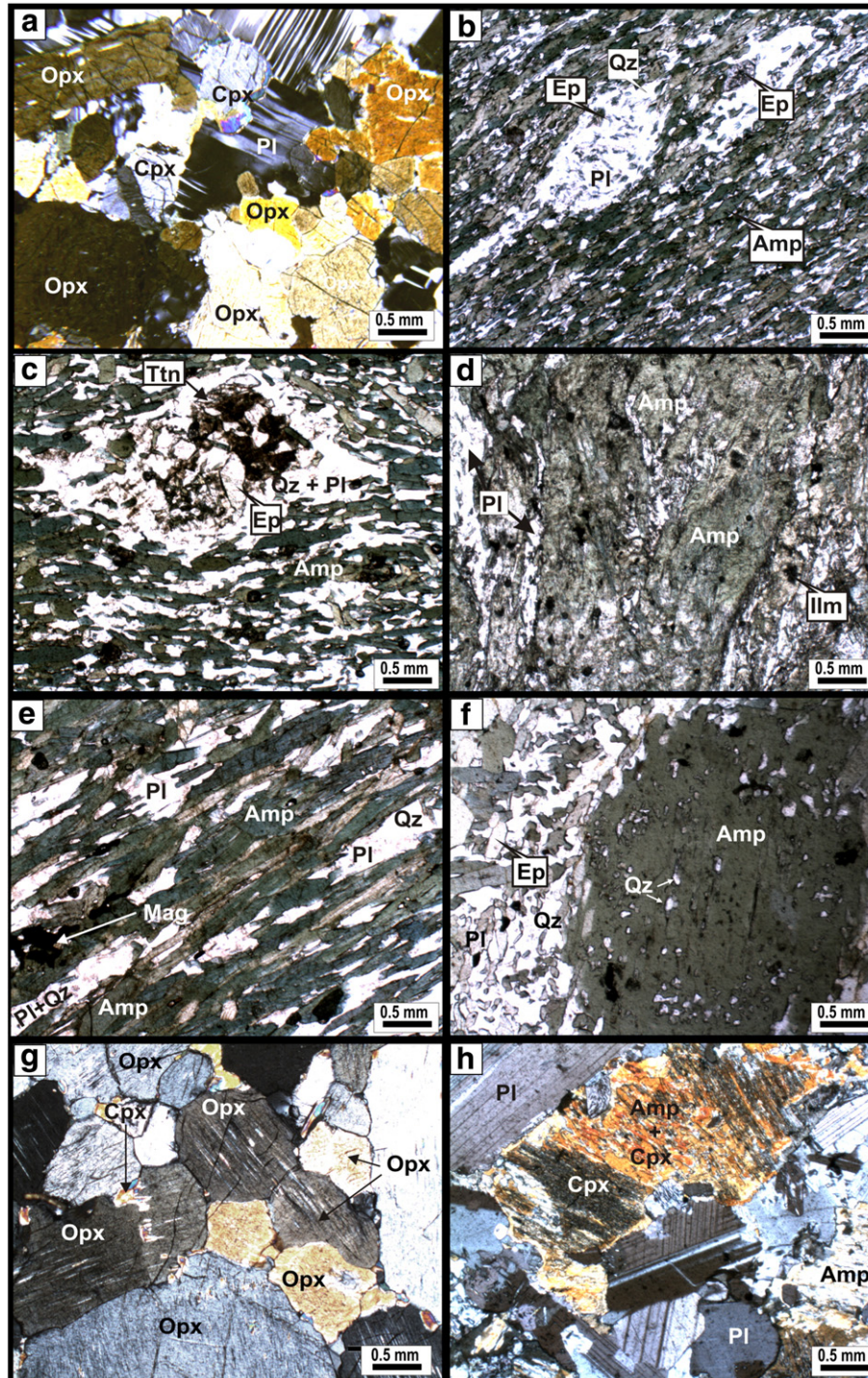
Fig. 8. Photomicrographs of mafic–ultramafic rocks (see Table 1). (a) Mafic granulite with granoblastic texture; (b) fine-grained amphibolite with stretched amygdules; (c) fine-grained amphibolite showing amygdule filled by Pl + Ep + Qz + Ttn; (d) amphibole rich-amphibolite with nematoblastic sigmoidal texture; (e) amphibole rich-amphibolite with penetrative foliation; (f) porphyroblastic amphibolite with small inclusion of quartz in amphibole; (g) ultramafic rock with granoblastic texture; (h) metagabbro with granoblastic texture. Plane polarized light (b, c, d, e, f) and cross-polarized light (a, g, h). Abbreviations: Ep—epidote; Ilm—Ilmenite; Pl—plagioclase; Qz—quartz, Cpx—clinopyroxene, Opx—orthopyroxene, Amp—amphibole; Ttn—titanite; Mag—magnetite.

correlation coefficient (R) <0.75 were regarded as mobile (Polat et al., 2004) and will not be used for petrogenetic interpretation. Therefore, we have assessed the effect of alteration on these elements in all sample mafic–ultramafic rocks. The abundance of the elements Si, K, Na, Sr and Ba show moderate variations (e.g., $K_2O = 0.13$–1.2 wt.%; $Na_2O = 0.33$–3.8 wt.%; Sr = 71–301 ppm and Ba = 20–420 ppm), which do not correlate well with Zr abundances (Fig. 10), and show weak correlations with

MgO contents (Appendix B — Fig. 1). Accordingly, these elements were screened out and not used for petrogenetic interpretation.

On the diagrams of Zr vs. Ti, Nb, Y and REE, most samples display systematic correlation consistent with a relatively low mobility of these elements in the Trincheira mafic–ultramafic rocks (Fig. 10). Similarly, despite its weak dispersion, there is a good correlations for these elements on MgO variation diagrams (Appendix B —
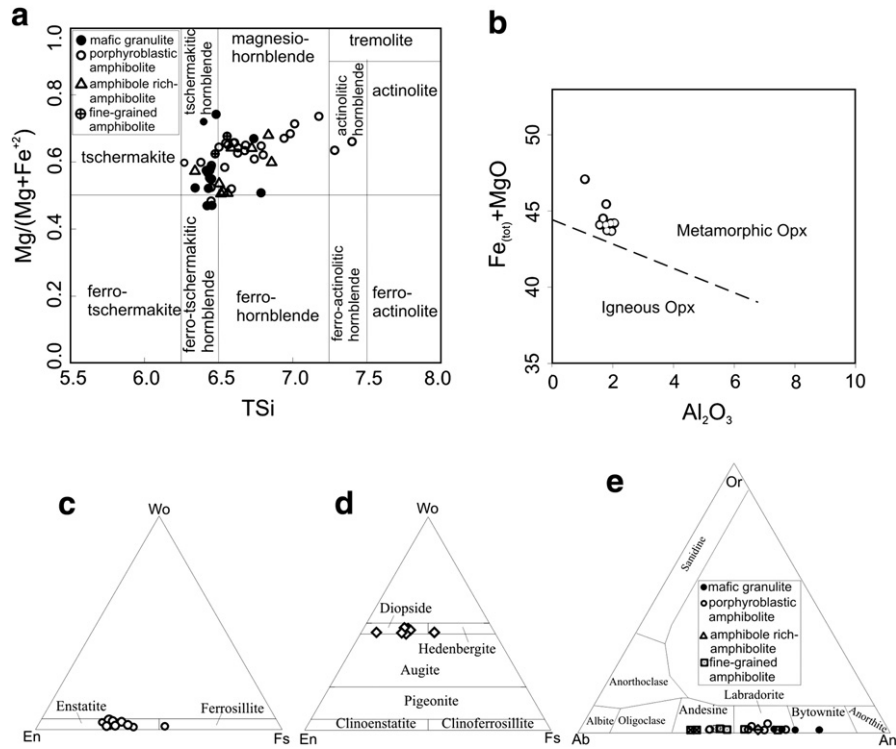
Fig. 9. (a) Compositional ranges of Ca-amphiboles from the Trincheira mafic–ultramafic Complex, expressed in the classification diagram of Leake (1978); (b) orthopyroxene compositions plotted in Fe(tot) + MgO x Al_2O_3 diagram of Bhattacharyya, (1971); (c and d) compositional variability of the composition of orthopyroxene and clinopyroxene from Trincheira mafic–ultramafic rocks, expressed in the diagram wollastonite–enstatite–ferrosilite; (e) chemical classifications of plagioclase in Or–Ab–An diagram.

Fig. 1). In addition, the evidence suggesting low mobility of Ti, Nb, Zr, Th and REE (except Ce) includes the following: (1) Th–Nb–La–Gd inter-element relationships do not correlate with loss on ignition (LOI) (Appendix B — Fig. 2); (2) the samples have consistent and coherent primitive mantle-normalized trace element patterns (Fig. 11). Thus, these elements are widely considered to be immobile and have not been significantly affected by post-magmatic alteration, and variation in their abundances can be attributed to olivine and/or pyroxene fractionation.

There is no evidence for any crustal contamination, according to initial Sr–Nd composition, by significantly older rocks in the Trincheira Complex (Rizzotto et al. unpublished data). Likewise, the absence of xenocrystic zircons in the Trincheira mafic–ultramafic rocks is also consistent with the absence of the continental crust in their geodynamic setting. The granitoids and felsic dykes in the region are younger than the Trincheira mafic–ultramafic rocks.

Most of mafic–ultramafic rocks plot in the basalts field on a Zr/Ti versus Nb/Y diagram, and only three samples are basaltic andesite composition (Fig. 12a). In variation diagrams with Zr (Fig. 10), mafic–ultramafic rocks show collinear trends for the HFSE, REE and transition metals, indicating their comparable composition. The mafic–ultramafic rocks were divided into five main groups (mafic–ultramafic cumulates are not shown), depending on the chemical characteristics of trace elements when normalized to chondrite and primitive mantle, according to Hofmann (1988) and Sun and McDonough (1989), respectively (Fig. 11, Table 2).

4.2.1. Fine-grained amphibolites

Fine-grained amphibolites are characterized by variable contents of SiO_2 and MgO; high Fe_2O_3 and Al_2O_3; moderate TiO_2 and CaO; and Mg# ranging from 34 to 52. Al_2O_3/TiO_2 ratios are sub-chondritic, whereas Ti/Zr and Zr/Y range from sub-chondritic to super-chondritic (Table 2 and Online Table 2). Additionally, the

fine-grained amphibolites show: (1) weak depletion to slightly fractionated LREE patterns (La/Sm$_{cn}$ = 0.62–1.15); near-flat REE patterns (La/Yb$_{cn}$ = 0.74–1.40); (2) flat to weak enrichment HREE pattern (Gd/Yb$_{cn}$ = 1.1–1.4) with moderate negative Nb, Ti, Zr anomalies; and no negative Eu anomalies (Fig. 11a–b, Table 2).

4.2.2. Amphibole rich-amphibolites

Amphibole rich-amphibolites have higher contents of MgO and Fe_2O_3, but low Zr and Ni and moderate to variable SiO_2, CaO and TiO_2 contents compared to modern average mid-ocean ridge basalt (MORB) (see Hofmann, 1988). Their Mg# range from 37 to 62 and their Al_2O_3/TiO_2 ratios are slightly sub-chondritic, whereas the Zr/Y ratios are sub-chondritic to slightly super-chondritic and Ti/Zr ranges from sub-chondritic to super-chondritic (Table 2 and Online Table 2). On chondrite and primitive mantle-normalized diagrams they have: (1) weak to moderate fractionation LREE patterns (La/Sm$_{cn}$ = 0.85–1.27; La/Yb$_{cn}$ = 0.86–2.17); slight fractionation HREE patterns (Gd/Yb$_{cn}$ = 1.02–1.67); moderate to large negative Nb, Ti, Zr anomalies; and very weak or absent negative Eu anomalies (Fig. 11c–d, Table 2).

4.2.3. Porphyroblastic amphibolites

Porphyroblastic amphibolites have Zr/Y (1.9–3.0) ratios comparable to modern tholeiitic basalts (Zr/Y = 1.3–3.1) (Barrett and MacLean, 1994). They have Mg# ranging from 52 to 62 and small variations of SiO_2, TiO_2, Fe_2O_3, Al_2O_3, MgO, Zr and REE contents (Fig. 8 and Table 2). The Al_2O_3/TiO_2 ratios are slightly sub-chondritic, whereas the Zr/Y ratios are sub-chondritic to slightly super-chondritic. The Ti/Zr ratio ranges from sub-chondritic to super-chondritic.

On the chondrite and primitive mantle-normalized diagrams, they have: (1) near-flat total REE patterns, slight depletion LREE patterns (La/Sm$_{cn}$ = 0.50–1.0); near-flat HREE patterns (Gd/Yb$_{cn}$ = 0.93–1.4);

Table 2

Representative major (wt.%) and trace element (ppm) concentrations and significant element ratios for mafic–ultramafic rocks. Major elements oxides in wt.%. FeO_t is total Fe expressed as Fe^{2+}. Mg# $= 100$ Mg/(Mg $+ Fe^{2+}$) assuming Fe_2O_3/FeO $= 0.15$. LDL $=$ lower than detection limit.

	Fine-grained amphibolites		Amphibole-rich amphibolites		Porphyroblastic amphibolites		Mafic granulites		Ultramafic cumulus (metapyroxenites)		Mafic cumulus (metagabbros)	
	GR 730	GR 738	NM 141	NM 54	GR 694	GR 710	GR 558	SJ 2562	GR-759	GR-760	GR-18	GR-761
$SiO_{2(wt.\%)}$	49.74	48.94	50.34	46.10	48.06	46.90	47.88	48.57	47.27	49.11	46.46	48.94
TiO_2	1.30	1.50	1.13	1.44	1.02	1.08	1.65	1.27	0.42	0.50	0.58	0.23
Al_2O_3	16.32	13.85	14.58	15.09	14.01	15.15	15.74	15.68	6.67	6.48	16.72	20.03
Fe_2O_3	11.42	13.47	12.84	11.33	11.68	12.88	12.98	12.30	11.38	11.79	9.71	6.31
MnO	0.19	0.21	0.20	0.15	0.29	0.20	0.20	0.19	0.19	0.18	0.18	0.14
MgO	5.65	7.51	6.55	9.34	7.22	7.89	6.26	6.90	19.16	19.24	10.51	7.98
CaO	11.44	9.76	10.22	12.50	12.57	10.99	11.18	11.30	8.85	7.58	12.93	13.08
Na_2O	2.60	2.94	2.80	2.36	2.27	1.88	2.54	2.39	0.38	0.33	1.49	1.99
K_2O	0.33	0.28	0.43	0.27	0.15	0.12	0.26	0.20	0.07	0.05	0.18	0.09
P_2O_5	0.15	0.17	0.24	0.12	0.107	0.12	0.16	0.12	0.02	0.10	0.06	0.01
LOI	0.60	1.10	0.60	1.20	2.40	2.50	0.90	0.80	4.90	3.90	1.10	1.00
Total	99.79	99.77	99.94	99.97	99.81	99.76	99.74	99.77	99.62	99.61	100	99.81
Mg#	49	52	50	62	55	55	49	53	77	76	68	71
Sc (ppm)	42	54	45	37	35	38	42	44	38	27	29	39
V	283	377	279	229	230	242	334	283	128	145	192	122
Cr	274	260	55	328	171	178	205	281	1875	1608	294	123
Co	45	50	47.3	53.1	48.4	57	50.4	51.5	70.7	75.9	61.2	34.1
Ni	64	93	58	171	100	114	69	70	461	546	294	36
Ga	18	17	18.1	15.4	15.9	15.4	19.2	17.7	8.8	8.8	14.4	16.2
Rb	6	8	7.7	14.4	1.8	3.8	4.2	3.8	2.8	2.4	4.4	1
Sr	164	101	299.4	250.6	178.5	158.1	207.3	211.1	55.6	71.9	165.6	301.1
Y	33.7	35.8	28	33.4	18.7	19.7	32.3	25.5	24.3	21.5	15.3	8.5
Zr	104.5	87.5	78	78.3	47.2	58.2	98.4	60.8	63.3	56.7	30.2	10.2
Nb	3.8	4.5	2.3	0.9	1.2	1	2.1	1.3	3.0	2.6	0.9	0.5
Ba	97	60	138.9	112.6	32	32	60	29	77	90	32.2	33
Ta	0.3	0.3	0.2	0.2	0.05	0.05	0.1	0.08	0.1	0.1	0.8	LDL
Th	0.8	0.8	1.3	0.5	0.1	0.1	0.3	0.2	0.8	1.5	0.4	0.16
Hf	3.4	2.9	2.2	2.7	1.5	1.3	2.9	1.8	2.1	1.5	1	0.2
U	0.4	0.2	0.4	LDL	LDL	LDL	0.2	0.1	0.3	0.6	0.3	LDL
La	6.2	3.6	5.9	2.6	2.3	2	4.4	2.9	8.4	11	1.6	1.7
Ce	16.4	8.4	15.3	8.6	6.2	7.6	14.2	9.5	13	19.7	4.3	3.7
Pr	2.6	1.82	2.26	1.65	1.13	1.28	2.35	1.56	3.57	3.1	0.71	0.58
Nd	12.9	10.7	11.1	10.3	6.1	9.5	12.2	8.7	17	13.9	3.4	3.3
Sm	3.89	3.76	3.1	3.8	1.92	2.57	3.94	2.79	4.14	3.19	1.2	1.08
Eu	1.27	1.39	1.1	1.46	0.81	0.95	1.46	1.17	1	0.82	0.59	0.56
Gd	4.89	5.24	3.92	4.95	2.65	2.99	5.28	3.96	4.06	3.41	1.96	1.27
Tb	0.93	0.97	0.65	0.93	0.52	0.57	0.94	0.71	0.73	0.57	0.38	0.25
Dy	5.8	6.12	4.31	6.31	3.08	3.79	5.39	3.92	4.47	3.55	2.5	1.43
Ho	1.23	1.32	0.97	1.33	0.69	0.76	1.12	0.88	0.85	0.74	0.52	0.33
Er	3.51	3.83	2.91	3.91	2.02	2.29	3.43	2.58	2.32	2	1.69	0.89
Tm	0.55	0.56	0.44	0.57	0.32	0.29	0.51	0.40	0.35	0.3	0.22	0.14
Yb	3.39	3.47	2.57	3.31	1.9	2.14	3.15	2.40	2.14	1.79	1.36	0.92
Lu	0.51	0.53	0.4	0.49	0.29	0.26	0.49	0.37	0.31	0.28	0.24	0.14
La/Yb_{cn}	1.31	0.74	1.65	0.56	0.87	0.67	1	0.87	2.82	4.41	0.84	1.33
La/Sm_{cn}	1.03	0.62	1.15	0.44	0.77	0.5	0.72	0.67	1.31	2.23	0.86	1.02
Gd/Yb_{cn}	1.19	1.25	1.26	1.24	1.15	1.16	2.63	2.42	1.57	1.58	1.19	1.14
$(Eu/Eu^*)_{cn}$	0.89	0.96	0.92	1.03	1.1	1.05	0.98	1.08	0.75	0.76	1.18	1.46
Al_2O_3/TiO_2	12.55	9.23	12.90	10.48	14	14	10	12	16	29	29	87
Zr/Y	3.1	2.44	2.79	2.34	2.5	3.0	3.05	2.38	2.60	1.97	1.97	1.20
Ti/Zr	75	103	87	110	130	111	101	125	40	53	115	135
$(Nb/Nb^*)_{pm}$	0.06	0.13	0.02	0.06	0.42	0.40	0.13	0.18	0.04	0.01	0.11	0.15
$(Zr/Zr^*)_{pm}$	0.10	0.10	0.11	0.09	0.19	0.11	0.10	0.12	0.04	0.06	0.35	0.14
$(Ti/Ti^*)_{pm}$	0.08	0.08	0.13	0.08	0.21	0.17	0.11	0.15	0.04	0.08	0.20	0.21

Notes: $Eu/Eu^* = (Eu)_{cn}/[(Sm)_{cn} + (Gd)_{cn}]^{1/2}$; $Nb/Nb^* = Nb_{pm}/(Th_{pm} \times La_{pm})$; $Ti/Ti^* = Ti_{pm}/(Tb_{pm} \times Dy_{pm})$; $Zr/Zr^* = Zr_{pm}/(Nd_{pm} \times Sm_{pm})$.

moderate to large negative Nb, Ti, and Zr anomalies; and no Eu (Eu/Eu* = 0.96–1.12) anomalies (Fig. 11e–f and Table 2).
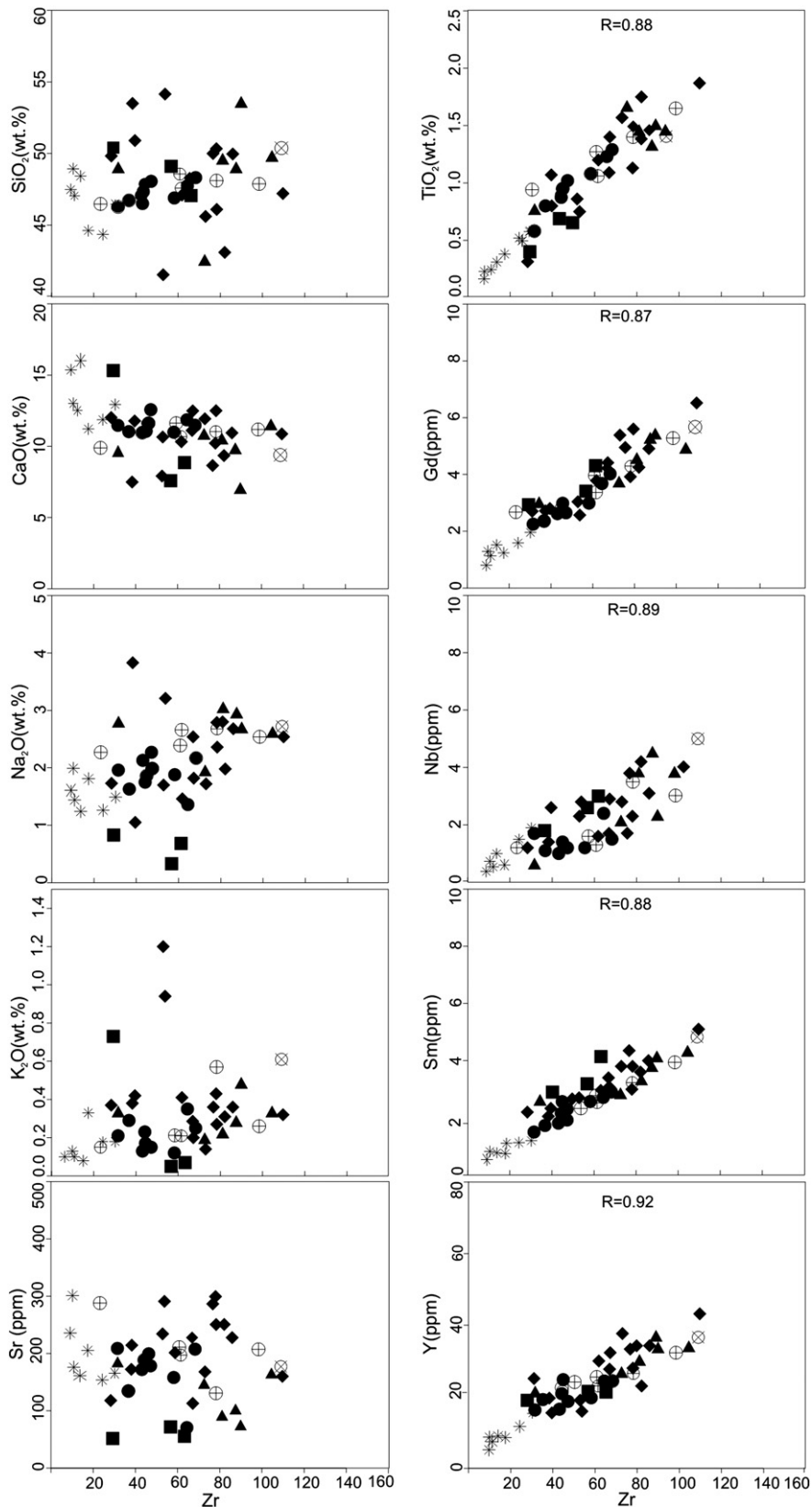
4.2.4. Mafic granulites

Mafic granulites are chemically very similar to porphyroblastic amphibolites. They are compositionally uniform in SiO_2, Fe_2O_3, CaO, MgO, Al_2O_3 and TiO_2 contents, while their Mg# range from 49 to 60. There is a large variation in Ni, and moderate variations in Co, V, Zr, Y and REE concentrations (Table 2). The Al_2O_3/TiO_2 ratios are sub-chondritic, whereas the Ti/Zr ratios are sub-chondritic to super-chondritic. In addition, the Zr/Y ratios are super-chondritic (Table 2 and Online Table 2). On chondrite and primitive mantle-normalized diagrams they have:

(1) slightly depleted LREE patterns ($La/Sm_{cn} = 0.67$–0.98); flat to slightly fractionated HREE patterns; large negative Nb, Ti, and Zr anomalies; and no Eu anomalies (Fig. 11g–h and Table 2).

4.2.5. Mafic–ultramafic cumulates

The mafic–ultramafic cumulates were divided into two groups: (a) those with pyroxene rich-cumulates and (b) those with plagioclase rich-cumulates. The first show variable SiO_2, Fe_2O_3 and CaO; high MgO (16.3–19.2 wt.%); and low Al_2O_3 and TiO_2 contents. Their Mg# range from 76 to 80. Additionally, the first group has high Ni (423–546 ppm) and Cr (1608–3770 ppm) and moderate Co, V, Zr, Y and REE contents (Table 2 and Online Table 2). The Al_2O_3/TiO_2

Fig. 10. Variation diagrams for a selected element plotted against the immobile element, Zr. Symbols: 4 — fine-grained amphibolite; ♦ — amphibole rich-amphibolite; ● porphyroblastic amphibolite; ⊕ — mafic granulite; ✳ — plagioclase cumulus; ■ pyroxene cumulus; ⊗ — gabbro.

(13–16) and Ti/Zr (40–82) ratios are sub-chondritic, whereas the Zr/Y (1.5–2.6) ratios are sub-chondritic to super-chondritic. In addition, they display the following trace element characteristics in chondrite and primitive mantle-normalized diagrams: (1) LREE enriched patterns;

moderately fractionated HREE patterns; large negative Nb, Ti, and Zr anomalies; and variably negative Eu anomalies (Table 2).

In comparison to pyroxene rich-cumulates, plagioclase rich-cumulates have similar SiO_2 but lower Fe_2O_3, MgO and TiO_2 and
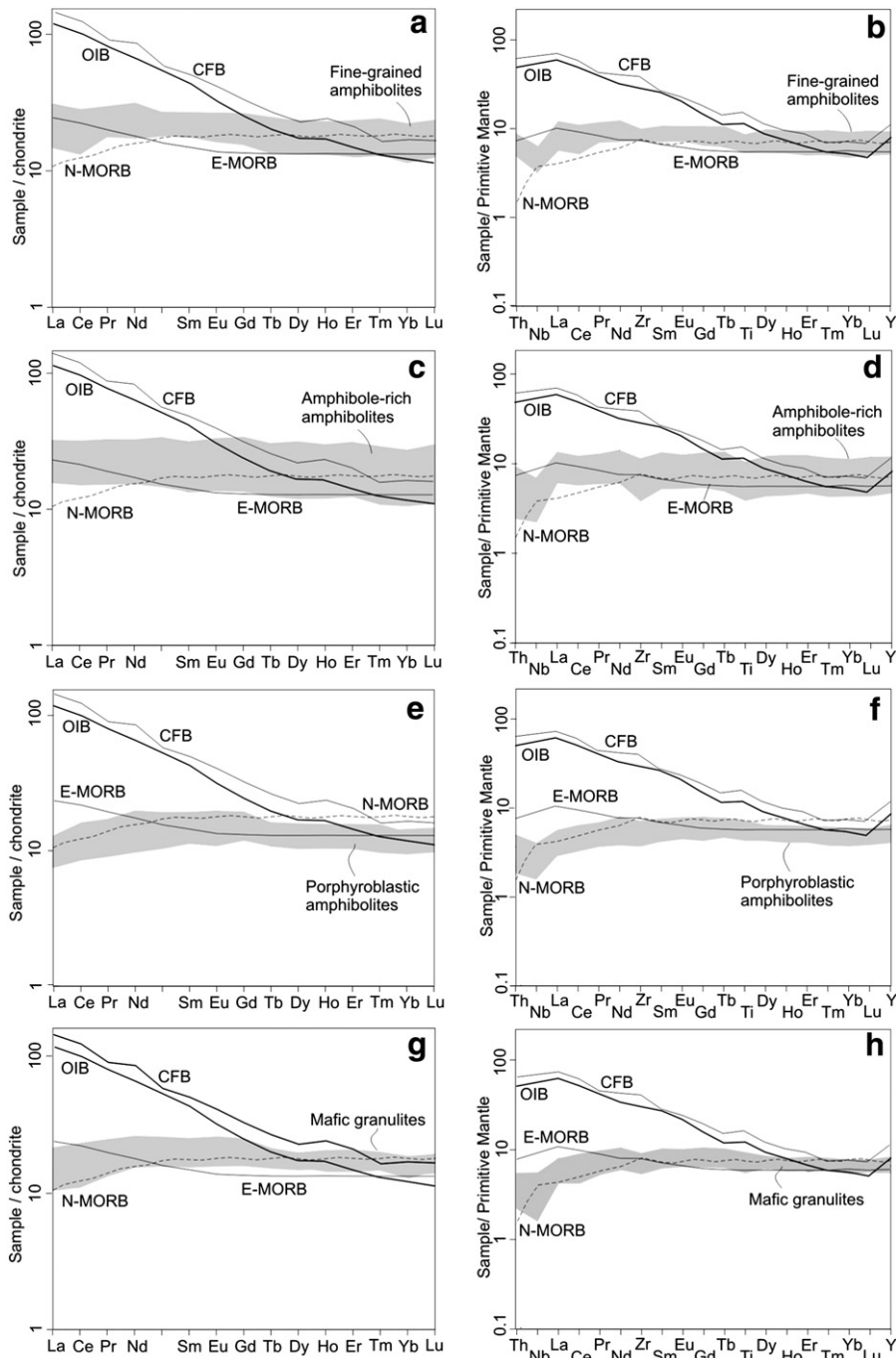
Fig. 11. Chondrite-normalized REE and primitive mantle-normalized trace element patterns for mafic–ultramafic rocks. Chondrite normalization values are from Sun and McDonough (1989) and primitive mantle normalization values are from Hofmann (1988). N-MORB, E-MORB, OIB e CFB standards for comparison.

higher CaO and Al_2O_3 contents. Their Mg-numbers are slightly lower, ranging from 68 to 79. They display lower and variable Ni and Cr; low Co, V, and Zr; and variable Y contents (Table 2 and Online Table 2). The plagioclase rich-cumulates also have Al_2O_3/TiO_2 and Ti/Zr ratios that are super-chondritic, while the Zr/Y ratios are sub-chondritic.

On chondrite and primitive mantle-normalized diagrams, they have: (1) near-flat LREE patterns; slightly fractionated HREE patterns; pronounced negative Nb, Ti, and Zr anomalies; and moderately positive Eu anomalies (Table 2 and Online Table 2).

5. Geodynamic setting and petrogenesis

This study documents an association of mafic–ultramafic rocks that were deformed, metasomatized and metamorphosed during the development of an accretionary orogen. Its extrusive rocks are predominantly massive basalts (now fine-grained amphibolites). Together with porphyroblastic amphibolites, mafic granulites, ultramafic rocks, chert, BIFs, pelites, psammitic and smaller proportion calc-silicate rocks, this association represents an ophiolitic sequence. While the rocks do not outcrop continuously due to the thick weathered material and the development of lateritic crusts in the tropical weather conditions that are characteristic of the hot and humid Amazon region, a continuous phase of deformation, including isoclinal folding and metamorphism of the granulite-amphibolite facies have been recognized. However, amygdaloidal, cumulate and layered magmatic structures have been preserved in areas of low strain in the rocks that comprise the Trincheira Complex. The presence of these primary structures provides a unique opportunity to study the characteristics of hydrothermal alteration, magma
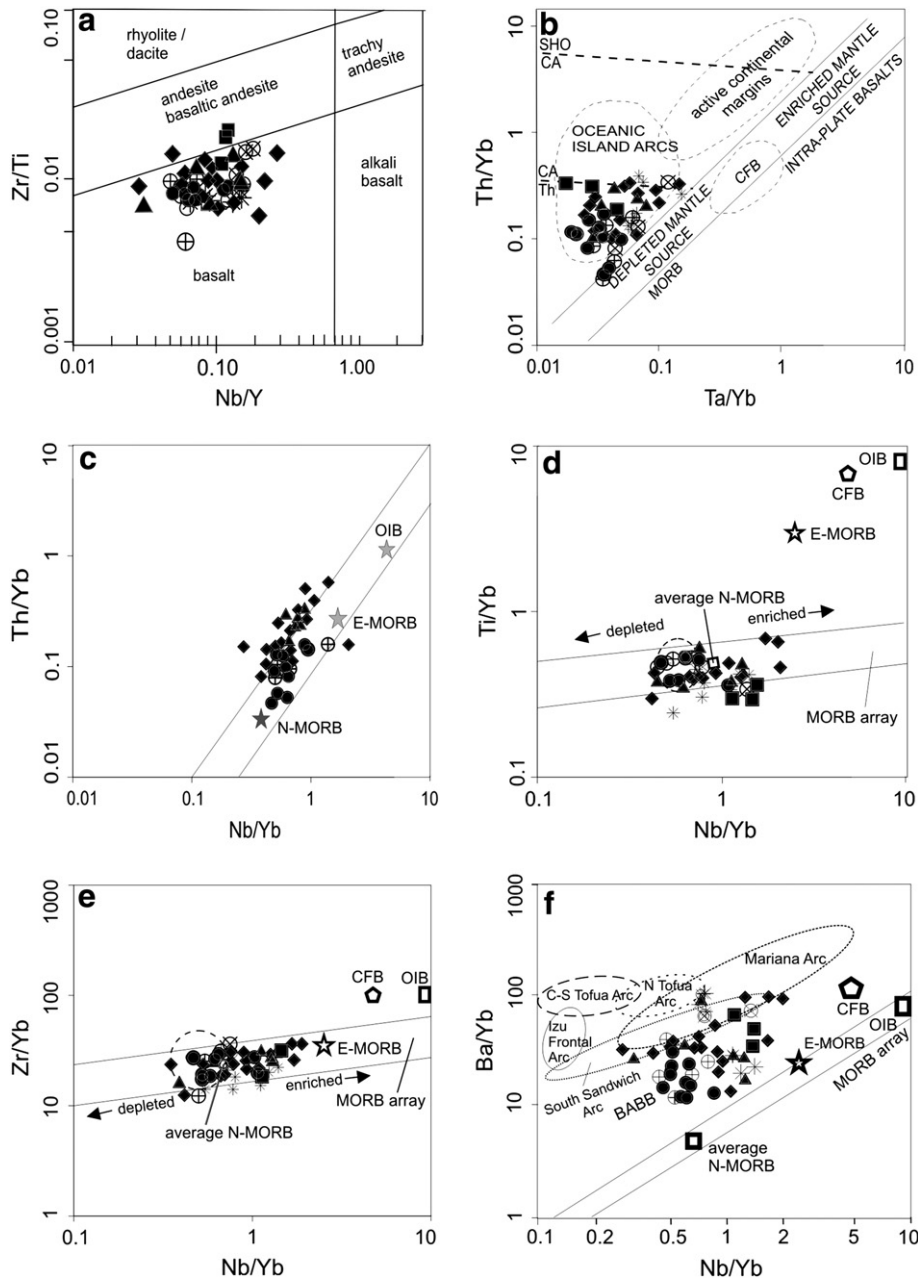
Fig. 12. (a) Distribution of mafic–ultramafic rocks of the Trincheira Complex, which occupy predominantly the field of basalts. Diagram modified from Pearce, 1996; (b) Th/Yb versus Ta/Yb and (c) Nb/Yb plots to show the distribution of the mafic–ultramafic rocks of the Trincheira Complex compared with oceanic island basalts (OIB), basalts derived from depleted sources (MORB), enriched source (E-MORB), uncontaminated intracontinental plate basalts and basalts derived from active continental margins; (d–e) distribution of samples of mafic granulites and porphyroblastic amphibolites (dotted area) in the field delimited by back-arc basin basalts of Pearce and Peat (1995); (f) distribution of samples of porphyroblastic amphibolites and mafic granulites in the field of BABB; and fine-grained amphibolites and amphibole rich-amphibolites in arc environment defined by Pearce and Stern (2006).

genesis and geodynamic processes. In this way, magmatism in the back-arc basins appears to result from the same basic processes responsible for the production of mid-ocean ridge basalt (MORB), or rifting of the oceanic crust leads to the passive uplift and partial melting of the upper mantle. Therefore, in many compositional aspects, back-arc basin basalts (BABB) are similar to MORBs (Taylor and Martinez, 2003). In detail, however, the evolution of back-arc basins is closely related to the processes of plate subduction, and the magmatism of back-arc basins is chemically and physically more variable than the magmatism generated at mid-ocean ridges. Specifically, the center of the spreading back-arc basin is positioned relatively close to active volcanic arcs and trench, and thus they are inevitably influenced by "components" derived from the subducted slab. It is believed that the water derived from the dehydration of the subducted slab should be the main carrier of such components,

and many studies have shown that the role and methods of transport by water and fusion differ systematically, mainly in back-arc basins and on mid-ocean ridges (Pearce and Stern, 2006).

The mafic–ultramafic rocks of Trincheira Complex represent mid-ocean ridge basalts (MORB) and island arc tholeiites. In general, the HFSE concentrations in the volcano-plutonic rocks of the Trincheira Complex are lower than those of modern N-MORBs (Table 2), indicating that the Mesoproterozoic mantle that originated the rocks of Trincheira Complex was more depleted in these elements when compared to modern N-MORB upper mantle. In addition, the mafic–ultramafic rocks have low Ni contents, which suggests that they are not derived from primary magmas that have undergone the fractionation of olivine.

The chemical characteristics presented above indicate that fine-grained amphibolites and amphibole rich-amphibolites, on the one

hand, and porphyroblastic amphibolites and mafic granulites, on the other, show specific characteristics of trace elements and REE, suggesting different sources and petrogenetic origins for these spatially and temporally associated groups of rocks. However, as a whole, the chemical differences when comparing the concentrations of REE and trace elements are subtle. Both groups show collinear trends of trace elements, HFSE, REE and transition metals in Zr variation diagrams showing broadly similar compositions (Fig. 10 and Table 2). However, when observed in detail, there are small differences between the groups formed by fine-grained amphibolites and amphibole rich-amphibolites. These trace element patterns show weak enrichment in LREE, enrichment in LILE (e.g., Rb, Ba, Sr and K) and a strong depletion of HFSE (e.g., negative Nb, Ti and Zr anomalies) consistent with a subduction zone geochemical signature (Saunders et al., 1991; Hawkesworth and Hooper, 1993; Pearce and Peate, 1995).

Additionally, the strong signature of the arc is evidenced by the enrichment of Pb and LILE relative to HFSE, which would involve a substantial amount of the subduction components having been present in the mantle source during the generation of fine-grained amphibolites and amphibole rich-amphibolites.

The igneous activity in island-arcs and back-arc basins are similar in some respects, although arc crustal growth is dominantly thickening due to the accumulation of lava and intrusion by magmatic underplating, while the crustal growth in the back-arc basin is caused by seafloor spreading (Hawkins et al., 1994). Flows of the intra-oceanic arc are characterized by high Ba/La and low Ce/Pb, combined with low $(La/Yb)_{cn}$ and moderate K/Rb ratios.

When studying suites of subduction-related basalts, Pearce (1982) found bivariate diagrams based on trace elements ratios to be useful in separating subduction-related from mantle components in the petrogenesis of the magmas. Fig. 12b is such a diagram, showing the variations of Th/Yb versus those of Ta/Yb. Compared to mid-ocean ridge basalts (MORB) and uncontaminated intra-plate basalts, the majority of the Trincheira Complex data plot within the field defined by oceanic island-arc basalts, where fine-grained amphibolites and amphibole-rich amphibolites show higher Th/Yb ratios in relation to mafic granulites and porphyroblastic amphibolites, presumably reflecting the influence of subduction-zone fluids enriched in Th in their petrogenesis. In addition, the MORB affinity for mafic granulites and porphyroblastic amphibolites and the island arc-related character of the fine-grained amphibolites and amphibole-rich amphibolites are well demonstrated on a Nb/Yb–Th/Yb diagram (Fig. 12c). The MORB and OIB domains form a diagonal mantle array on this discriminant diagram, whereas magmas that have a subduction component are displaced to higher Th/Yb values.

In the remaining two discriminant diagrams (HFSEs), mafic granulites and porphyroblastic amphibolites show weak depletion in LREE and variable degrees of depletion of HFSE (Nb, Ti, and Zr), as shown in the diagrams of conservative elements in subduction systems (Pearce and Peate, 1995) (Fig. 12d and e) and similarly to modern back-arc basin basalts (BABB). Likewise, the diagrams show the influence of components derived from the subducted slab as enrichments in Rb, Ba and Sr, but lower quantities to fine-grained amphibolites and amphibole rich-amphibolites. The elements with low ionic potential are most readily mobilized by a fluid phase, and their enrichment in island-arc basalts has been attributed to the metasomatism of their mantle source region by hydrous fluids derived from the subducted oceanic crust.

On Fig. 12f most samples of mafic granulites and porphyroblastic amphibolites of the Trincheira Complex are plotted in the BABB field, while the fine-grained amphibolites and amphibole-rich amphibolites are distributed in the field delimited by the rocks' arc setting, some of which are transitional to BABB.

5.1. Trincheira Complex: implications for Columbia supercontinent

Ophiolites represent fragments of upper mantle and oceanic crust that were incorporated into mountain belts during subduction–accretion

events. They are generally found along suture zones in both collisional-type and accretionary-type orogenic belts that mark major boundaries between amalgamated plates or accreted terranes (Lister and Forster, 2009). Thus, subduction-related lithosphere and ophiolites develop during the closure of ocean basins. Some of the main processes of ophiolite genesis and emplacement overlap in time with major orogenic events that led to the construction of supercontinents. Likewise, the formation of supercontinents is commonly explained by the coalescence of numerous continental fragments (cratons, microcontinents) along sutures formed by the closure of ocean basins between them (Unrug, 1992). Examples of Phanerozoic orogenic events include the Famatian and Caledonian (Baltica–Laurentia collision) orogens in the early Paleozoic, which collectively formed the Gondwana and Laurasia supercontinents, and the Appalachian–Hercynian and Altaid–Uralian orogens later in the Paleozoic, which built the Pangea supercontinent (Moores et al., 2000). These Phanerozoic ophiolites commonly show MORB to IAT geochemical affinities. Similar tectonic processes probably occurred in the Proterozoic through which supercontinents were formed by the amalgamation of pre-existing continental masses, with the concomitant disappearance of the intervening oceans.

Many alternative configurations have been proposed for the Paleo- to Mesoproterozoic Columbia supercontinent, although its configuration is based on the available paleomagnetic data that are normally affected by large uncertainties, especially regarding paleolongitudes (Bispo-Santos et al., 2008; D'Agrella-Filho et al., 2012; Hou et al., 2008; Johansson, 2009; Kusky et al., 2007; Meert, 2002; Pesonen et al., 2003; Rogers and Santosh, 2002; Zhao et al., 2002, 2004, 2006). The possibility that this phase of Earth history involved assembly of a supercontinent was suggested by the abundance of orogenic activity between about 1.8 Ga and 1.6 Ga (Rogers and Santosh, 2004). According to previous work there is considerable to evidence show that, following its assembly at circa 1.8 Ga, the Columbia supercontinent underwent long-lived (1.8–1.2 Ga) accretion along some of its continental margins. In our view, the configuration of Columbia implies subduction-related outgrowth along the southwestern margin of the Amazon craton around 1.47 to 1.35 Ga.

The age and the character of the Paleo- to Mesoproterozoic belts of SW Amazon craton permit correlation with the Svecofennian domain and the Transcandinavian igneous belt within Baltica and also with the Mid-continent region of Laurentia. These similarities led several authors to propose a possible link between the north-northeastern Amazon craton and southwestern Baltica (e.g., Cordani et al., 2009; Geraldes et al., 2001; Johansson, 2009; Sadowski and Bettencourt, 1996; Zhao et al., 2002, 2004, 2006). Both cratons show subduction-related accretionary belts, which evolved throughout the Mesoproterozoic at the margins of such contiguous cratonic nuclei. In contrast, paleomagnetic data presented by Bispo-Santos et al. (2008) and Pesonen et al. (2003) indicate that these cratons were not linked. New paleomagnetic data from D'Agrella-Filho et al. (2012) provides a test for the longevity of the previously proposed Columbia paleogeography and led the authors to suggest that the break-up of Columbia must have taken place before 1420 Ma. But the paleogeography of the Amazon craton closer to Baltica in the Mesoproterozoic is also allowed by the paleomagnetic data.

In this work, the recognition of the Trincheira ophiolite and suture significantly changes views on the evolution of the southern margin of the Amazon craton, and how it can influence the global tectonics and the reconstruction of the continents. It also modifies current ideas about Amazonia's role in plate reconstructions of the Columbia supercontinent.

The relation of Amazonia, Laurentia and Baltica is a key issue for the continental reconstruction of the Mesoproterozoic. The eastern margin of Laurentia was a site of continued continental-margin orogeny with subduction-related outgrowth. This outgrowth is well shown by the Yavapai, Labradorian and Mazatzal provinces of southwestern United States, which developed from ~1.8–1.5 Ga. The western part of the Amazon craton also underwent marginal growth from

~1.8–1.3 Ga, when subduction beneath Amazonia progressively formed the Rio Negro–Juruena and Alto Guaporé belts. The Alto Guaporé belt is partly formed by the small Paraguá crustal block that possibly was originally part of older continents. From ~1.47 Ga to 1.35 Ga compressional orogeny occurred along the southwestern margin of the Amazon craton, subduction below Amazonia followed by granulite-facies metamorphism. In our view, the juvenile rocks of the Trincheira Complex and related magmatic arcs (Rio Alegre terrane), dated between 1470 and 1350 Ma, could well correspond to the accreted intra-oceanic material that attests the existence of a large ocean that separated Amazonia from Laurentia. The final closure of the ocean was marked by the accretion of the Paraguá microcontinent around 1.35 Ga. Thus, the discovery of the Mesoproterozoic Trincheira ophiolite supplies important evidence for the existence of an oceanic basin on the southern margin of the Amazon craton, and demonstrates that the Amazon craton had its growth, first by accretion of oceanic crust and later by collision with Paraguá Block on its southwestern margin. Additionally, petrotectonic studies in the Trincheira Complex are consistent with a belt that grew along a northward dipping subduction zone through accretion of oceanic island arc and back-arc. Therefore, growth of the southwestern Amazon craton was through subduction-related magmatism during continued accretion of juvenile material in Mesoproterozoic times. This implies that in the Columbia supercontinent, at ~1.5–1.3 Ga, the southern margin of the proto-Amazon craton was not connected to any other continent, but was bordered by an active supra-subduction zone. This scenario can be related to the reconstruction of Paleo-Mesoproterozoic supercontinent Columbia proposed by Zhao et al. (2004). In contrast, D'Agrella-Filho et al. (2012), based on paleomagnetic data proposed the Columbia reconstruction at ~1460 Ma and suggest that there was no major ocean between the Paraguá Block and proto-Amazon craton at roughly this time. However, this new scenario for Mesoproterozoic Columbia supercontinent proposed by the authors mentioned above, does not address the oceanic lithosphere that existed between the proto-Amazon craton and Paraguá Block, represented by the Trincheira Complex.

Details on the life cycle duration of Columbia have yet to be reliably established. Therefore, any attempt to reconstruct the supercontinent must take into account the existence of oceanic crust during the Mesoproterozoic in the southern border of the proto-Amazon craton. Therefore, it is necessary paleomagnetic studies in this important belt of mafic–ultramafic rocks to better understand the paleogeographic reconstruction for the supercontinent that preceded Rodinia.

At about 1.35–1.25 Ga, in South America, Mesoproterozoic rapakivi granites younger than 1.35 Ga, such as the Teotônio Intrusive Suite (~1.34 Ga), Santo Antônio Intrusive Suite (~1.36 Ga), Alto Candeias Intrusive Suite (1.33 Ga), and associated intracontinental rifting represented by sedimentary and igneous rocks of the Nova Brasilândia Group (>1.25 Ga) (Bettencourt et al., 1999, 2010; Rizzotto, 1999), coupled with the intrusions of many mafic dike swarms and associated basaltic extrusions in other places worldwide marks a major episode of plate-wide extension and rifting, and signaled the final breakup of the Columbia supercontinent.

6. Conclusions

The Trincheira mafic–ultramafic Complex is composed of several disrupted, highly dismembered imbricate thrust slices forming an incomplete ophiolitic sequence. The sequence includes layered mafic–ultramafic cumulates and intrusive mafic–ultramafic and extrusive mafic rocks with an interbedded sedimentary clast-chemical sequence. The deformation is heterogeneous, as indicated by highly deformed zones adjacent to areas with poorly developed foliation or a partially preserved primary texture. Based on the characteristics of the field, petrographic, geophysical and geochemical, was suggested a division of the complex into three units: a) Lower Unit: layered mafic–ultramafic rocks (granulite-facies metamorphism): mafic granulites which has as

protolith olivine–orthopyroxenite, bronzitite, and websterite; b) Intermediate Unit: intrusive mafic rocks (amphibolite-facies metamorphism): banded amphibolites that has as protolith norite, gabbronorite, gabbro, anorthosite, gabbroanorthosite and rare plagiogranite; and c) Upper Unit: extrusive mafic rocks (amphibolite-facies metamorphism): fine-grained amphibolites (basalt massive and pillow) with intercalations of sedimentary sequence consisting of metachert (BIFs), calc-silicate rocks and aluminous schist/quartzite.

Metamorphism is pervasive. It attained temperatures of 820–853 °C and 680–720 °C for mafic granulites and amphibolites, respectively, and a pressure of 6.8 kbar.

The presence of layers of chert, BIFs and amygdaloidal basalt is consistent with an oceanic setting for the eruption of volcanic rocks and associated intrusions. Therefore, the analysis of the new geological and geochemical data presented here indicates that the mafic–ultramafic rocks of the Trincheira Complex have a hybrid mixture of MORB-like and arc-like element signatures and are part of a supra-subduction system formed by an intra-oceanic island arc and back-arc basin. Its fine-grained amphibolites and amphibole rich-amphibolites have a closer similarity to arc tholeiites, while the mafic granulites and porphyroblastic amphibolites are chemically compatible with the modern BABB. The participation of a subduction component is implicit in the high Rb, Sr, Ba and K contents in proportion to immobile elements (HFSE), such as Nb and Ta. The water derived from the dehydration of the subducted slab is the main carrier of such components. In summary, the behavior of trace elements suggests that the mantle source of lavas and intrusive of Trincheira Complex was affected by subduction components. This relict oceanic crust may represent a fragment of oceanic lithosphere that obducted during what remained of the collision of the Paraguá block with the western border of the Amazon craton during the Middle Mesoproterozoic period, between 1470 and 1350 Ma. This tectonic model explains many previously enigmatic features of the Precambrian history of this key craton, and discusses its role in the reconstruction of the Columbia supercontinent.

Acknowledgments

Appendix A. Supplementary data

Supplementary data to this article can be found online at doi:10.1016/j.lithos.2012.05.027.

References

Arndt, N.T., 1994. Archean komatiites. In: Condie, K.C. (Ed.), Archean Crustal Evolution. Elsevier, Amsterdam, pp. 11–44.
Arndt, N.T., Albarbde, E., Nisbet, E.G., 1997. Mafic and ultramafic magmatism. In: de Wit, M.J., Ashwal, L.D. (Eds.), Greenstone Belts. Clarendon Press, Oxford, pp. 233–254.
Barrett, T.J., MacLean, W.H., 1994. Chemostratigraphy and hydrothermal alteration in exploration for VHMS deposits in greenstones and younger volcanic rocks. In: Lenz, D.R. (Ed.), Alteration and Alteration Processes Associated with Ore-forming Systems. Geological Association of Canada, Short Course Notes, vol. 11, pp. 433–467.
Bettencourt, J.S., Tosdal, R.M., Leite Jr., W.B., Payolla, B.L., 1999. Mesoproterozoic rapakivi granites of Rondonia Tin Province, southwestern border of the Amazonian Craton, Brazil—I. Reconnaissance U–Pb geochronology and regional implications. Precambrian Research 95, 41–67.
Bettencourt, J.S., Leite Jr., W.B., Ruiz, A.S., Matos, R., Payolla, B.L., Tosdal, R.M., 2010. The Rondonian–San Ignacio Province in the SW Amazonian Craton: an overview. Journal of South American Earth Sciences 29, 28–46.

Bhattacharyya, C., 1971. An evaluation of the chemical distinctions between igneous and metamorphic orthopyroxenes. American Mineralogist 56, 499–506.

Bispo-Santos, F., D'Agrella-Filho, M.S., Pacca, I.I.G., Janikian, L., Trindade, R.I.F., Elming, S., Silva, J.A., Barros, M.A.S., Pinho, F.E.C., 2008. Columbia revisited: paleomagnetic results from the 1790 Ma Colíder volcanics (SW Amazonian Craton, Brazil). Precambrian Research 164, 40–49.

Boger, S.D., Raetz, M., Giles, D., Etchart, E., Fanning, C.M., 2005. U–Pb age data from the Sunsas region of eastern Bolivia, evidence for the allochtonous origin of the Paraguá Block. Precambrian Research 139, 121–146.

Brunsmann, A., Franz, G., Erzinger, Landwehr, D., 2000. Zoisite- and clinozoisite-segregations in metabasites (Tauern Window, Austria) as evidence for high-pressure fluid–rock interaction. Journal of Metamorphic Geology 18, 1–21.

Cann, J.R., 1970. Rb, Sr, Y, Zr and Nb in some ocean floor basaltic rocks. Earth and Planetary Science Letters 10, 7–11.

Cawood, P.A., Nemchin, A.A., Strachan, R., Prave, T., Krabbendam, M., 2007. Sedimentary basin and detrital zircon record along East Laurentia and Baltica during assembly and breakup of Rodinia. Journal of the Geological Society 164, 257–275.

Cawood, P.A., Kroner, A., Collins, W.J., Kusky, T.M., Mooney, W.D., Windley, B.F., 2009. Accretionary orogens through Earth history. Geological Society, London, Special Publications 318, 1–36.

Cordani, U.G., Teixeira, W., 2007. Proterozoic accretionary belts in the Amazonian Craton. In: Hatcher, R.D., Carlson Jr., M.P., McBride, J.H., Martinez Catalan, J.R. (Eds.), 4-D framework of continental crust: Geological Society of America Memoir, 200, pp. 297–320.

Cordani, U.G., Teixeira, W., D'Agrella-Filho, M.S., Trindade, R.I., 2009. The position of the Amazonian Craton in supercontinents. Gondwana Research 15, 396–407.

D'Agrella-Filho, M.S., Tohver, E., Santos, J.O.S., Elming, S.A., Trindade, R.I.F., Pacca, I.G., Geraldes, M.C., 2008. Direct dating of paleomagnetic results from Precambrian sediments in the Amazon Craton: evidence for Grenvillian emplacement of exotic crust in SE Appalachians of North America. Earth and Planetary Science Letters 267, 188–199.

D'Agrella-Filho, M.S., Trindade, R.I.F., Elming, S., Teixeira, W., Yokoyama, E., Tohver, E., Geraldes, M.C., Pacca, I.I.G., Barros, M.A.S., Ruiz, A.S., 2012. The 1420 Ma Indiavaí Mafic Intrusion (SW Amazonian Craton): paleomagnetic results and implications for the Columbia supercontinent. Gondwana Research. http://dx.doi.org/10.1016/j.gr.2012.02.022.

Dalziel, I.W.D., 1991. Pacific margins of Laurentia and East-Antarctica–Australia as a conjugate rift pair: evidence and implications for an Eocambrian supercontinent. Geology 19, 598–601.

Dilek, Y., Furnes, H., 2009. Structure and geochemistry of Tethyan ophiolites and their petrogenesis in subduction rollback systems. Lithos 113, 1–20.

Dilek, Y., Thy, P., Hacker, B., Grundvig, S., 1999. Structure and petrology of Tauride ophiolites and mafic dike intrusions (Turkey): implications for the Neo-Tethyan ocean. Geological Society of America Bulletin 111, 1192–1216.

Frei, R., Rosing, M., Waight, T.E., Krogstad, E.J., Storey, M., Ulfbeck, D.G., Albarde, E., 2002. Hydrothermal–metasomatic and tectono-metamorphic processes in the Isua greenstone belt (West Greenland): a multi-isotopic investigation of their effects on the Earth's oldest oceanic crustal sequence. Geochimica et Cosmochimica Acta 66, 467–486.

Geraldes, M.C., Van Schmus, W.R., Condie, K.C., Bell, S., Teixeira, W., Babinski, M., 2001. Proterozoic Geologic Evolution of the SW part of the Amazonian Craton in Mato Grosso State, Brazil. Precambrian Research 111, 91–128.

Hawkesworth, C.J., Hooper, P.R., 1993. Isotopic and geochemical constraints on the origin and evolution of the Columbia River Basalt. Journal of Petrology 34, 1203–1246.

Hawkins, J.W., Bloomer, S.H., Evans, C.A., Melchior, J.T., 1994. Evolution of intra-oceanic arc–trench systems. Tectonophysics 102, 174–205.

Hoffman, P.F., 1991. Did the breakout of Laurentia turn Gondwanaland inside-out? Science 252, 1409–1412.

Hofmann, A.W., 1988. Chemical differentiation of the Earth: the relationships between mantle, continental crust, and oceanic crust. Earth and Planetary Science Letters 90, 297–314.

Holland, T.J.B., Blundy, J., 1994. Non-ideal interactions in calcic amphiboles and their bearing on amphibole-plagioclase thermometry. Contributions to Mineralogy and Petrology 116, 433–447.

Hou, G., Santosh, M., Qian, X., Lister, G.S., Li, J., 2008. Configuration of the Late Paleoproterozoic supercontinent Columbia: insights from radiating mafic dyke swarms. Gondwana Research 14, 395–409.

Ishikawa, T., Nagaishi, K., Umino, S., 2002. Boninitic volcanism in the Oman ophiolite: implications for thermal conditions during transition from spreading ridge to arc. Geology 30, 899–902.

Jenner, G.A., Cawood, P.A., Rautenschlein, M., White, W.M., 1987. Composition of back-arc basin volcanics, Valu Fa Ridge, Lau Basin: evidence for a slab-derived component in their mantle source. Journal of Volcanology and Geothermal Research 32, 209–222.

Jochum, K.P., Arndt, N.T., Hofmann, A.W., 1991. Nb–Th–La in komatiites and basalts: constraints on komatiite petrogenesis and mantle evolution. Earth and Planetary Science Letters 107, 272–289.

Johansson, A., 2009. Baltica, Amazonia and the SAMBA connection — 1000 million years of neighbourhood during the Proterozoic? Precambrian Research 175, 221–234.

Keppie, D., Dostal, J., Ortega-Gutiérrez, F., Lopez, R., 2001. A Grenvillian arc on the margin of Amazonia: evidence from the southern Oaxacan Complex, southern Mexico. Precambrian Research 112, 165–181.

Kusky, T.M., Li, J., Santosh, M., 2007. The Paleoproterozoic North Hebei Orogen: North China craton's collisional suture with the Columbia supercontinent. Gondwana Research 12, 4–28.

Leake, B.E., 1978. Nomenclature of amphiboles. American Mineralogist 63, 1023–1052.

Lister, G., Forster, M., 2009. Tectonic mode switches and the nature of orogenesis. Lithos 113, 274–291.

Litherland, M., Annels, R.N., Appleton, J.D., Berrange, J.P., Bloomfield, K., Darbyshire, D.P.F., Fletcher, C.J.N., Hawkins, M.P., Klinck, B.A., Mitchell, W.I., O'Connor, E.A., Pitfield, P.E.J., Power, G., Webb, B.C., 1986. The geology and mineral resources of the Bolivian Precambrian Shield. Overseas Memoir British Geological Survey 9 (153 pp.).

Litherland, M., Annels, R.N., Darbyshire, D.P.F., Fletcher, C.J.N., Hawkins, M.P., Klink, B.A., Mitchell, W.I., O'Connor, E.A., Pitfield, P.E.J., Power, G., Webb, B.C., 1989. The Proterozoic of eastern Bolivia and its relationship to the Andean mobile belt. Precambrian Research 43, 157–174.

Ludden, J.N., Gélinas, L., Trudel, P., 1982. Archean metavolcanics from the Rouyn–Noranda district, Abitibi greenstone belt, Québec. 2. Mobility of trace elements and petrogenetic constraints. Canadian Journal of Earth Sciences 19, 2276–2287.

Meert, J.G., 2002. Paleomagnetic evidence for a Paleo-Mesoproterozoic supercontinent Columbia. Gondwana Research 5, 207–215.

Moores, E.M., Kellogg, L., Dilek, Y., 2000. Tethyan ophiolites, mantle convection, and tectonic "historical contingency": a resolution of the "ophiolite conundrum. In: Dilek, Y., Moores, E.M., Elthon, D., Nicolas, A. (Eds.), Ophiolites and Oceanic Crust: New Insights from Field Studies and Ocean Drilling Program: Geological Society of America Special Paper, 349, pp. 3–12.

Murton, B.J., Peate, D.W., Arculus, R.J., Pearce, J.A., Van Der Laan, S.R., 1992. Trace-element geochemestry of volcanic rocks from Site 786: the Izu–Bonin forearc. In: Fryer, P., Pearce, J.A., Stokking, L.B., et al. (Eds.), Proceedings of the Ocean Drilling Program, Scientific Results 125, 211–235.

Pearce, J.A., 1982. Trace element characteristics of lavas from destructive plate boundaries. In: Thorpe, R.S. (Ed.), Andesites. John Wiley and Sons, pp. 525–548.

Pearce, J.A., Cann, J.R., 1973. Tectonic setting of basic volcanic rocks determined using trace element analyses. Earth and Planetary Science Letters 19, 290–300.

Pearce, J.A., Peate, D.W., 1995. Tectonic implications of the composition of volcanic arc magmas. Annual Review of Earth and Planetary Science 23, 251–285.

Pearce, J.A., Stern, J.R., 2006. The Origin of Back-arc Basin Magmas: Trace Element and Isotopic Perspectives. In: Christie, D.M., Fisher, C.R., Lee, S.-M., Givens, S. (Eds.), Back-arc spreading systems: geological, biological, chemical, and physical interactions: AGU monograph, American Geophysical Union. Geophysical Monograph, Washington DC, pp. 63–86.

Pearce, J.A., Van Der Laan, S.R., Arculus, R.J., Murton, B.J., Ishii, T., 1992. Boninite and harzburgite from Leg 125 (Bonin–Mariana forearc): a case study of magma genesis during the initial stages of subduction. In: Fryer, P., Pearce, J.A., Stokking, L.B., et al. (Eds.), Proceedings of the Ocean Drilling Program, Scientific. Texas A&M University, College Station, pp. 623–659.

Pesonen, L.J., Elming, S., Mertanen, S., Pisarevsky, S., D'Agrella-Filho, M.S., Meert, J.G., Schmidt, P.W., Abrahamsen, N., Bylund, G., 2003. Palaeomagnetic configuration of continents during the Proterozoic. Tectonophysics 375, 289–324.

Polat, A., Kerrich, R., Wyman, D.A., 1998. The late Archean Schreiber–Hemlo and White River–Dayohessarah greenstone belts, Superior Province: collages of oceanic plateaus, oceanic arcs, and subduction–accretion complexes. Tectonophysics 289, 295–326.

Polat, A., Hofmann, A.W., Rosing, M.T., 2002. Boninite-like volcanic rocks in the 3.7–3.8 Ga Isua greenstone belt, West Greenland: geochemical evidence for intra-oceanic subduction zone processes in the early Earth. Chemical Geology 184, 231–254.

Polat, A., Hofmann, A.W., Appel, P.W.U., 2004. Geochemical diversity in volcanic rocks of the 3.7–3.8 Ga Isua Greenstone belt, southwest Greenland: implications for mantle composition. In: Eriksson, P.G., Altermann, W., Nelson, D.R., Mueller, W.U., Catuneanu, O. (Eds.), Tempos and Events in Precambrian Time. Development in Precambrian Geology, vol.12. Elsevier, pp. 74–88.

Puchtel, I.S., Hofmann, A.W., Mezger, K., Jochum, K.P., Shchipansky, A.A., Samsonov, A.V., 1998. Oceanic plateau model for continental crustal growth in the Archaean: a case study from the Kostomuksha greenstone belt, NW Baltic Shield. Earth and Planetary Science Letters 155, 57–74.

Rizzotto, G.J., 1999. Petrologia e geotectônica do Grupo Nova Brasilândia, Rondônia. MSc. Dissertation. Federal University of Rio Grande do Sul. Porto Alegre, Brazil, p. 131 (in Portuguese).

Rizzotto, G.J., 2010. Geologia e Recursos Minerais da Folha Pimenteiras (SD.20-X-D). Sistema de Informação Geográfica-SIG. CPRM, Rondônia, Brazil. 136 pp. (in Portuguese).

Rizzotto, G.J., Dehler, N., 2007. Arcabouço Estrutural Da Faixa Alto Guaporé e o Regime Tectônico do Ectasiano na Borda SW do Cráton Amazônico. XI Simpósio Nacional de Estudos Tectônicos, Natal. ANAIS XI Simpósio Nacional de Estudos Tectônicos (in Portuguese).

Rizzotto, G.J., Bettencourt, J.S., Teixeira, W., Pacca, I.G., D'Agrella-Filho, M.S., Vasconcelos, P.M., Basei, M.A.S., Onoe, A.T., Passarelli, C.R., 2002. Geologia e geocronologia da Suite Metamórfica Colorado e suas encaixantes, SE de Rondônia: implicações para a evolução mesoproterozóica do SW do Craton Amazônico. Revista do Instituto de Geociências USP: Série Científica, 2, pp. 41–55 (in Portuguese).

Rogers, J.J.W., Santosh, M., 2002. Configuration of Columbia, a Mesoproterozoic supercontinent. Gondwana Research 5, 5–22.

Rogers, J.J.W., Santosh, M., 2004. Continents and Supercontinents. Oxford University Press, New York. 289 pp.

Romanini, S.J., 2000. Programa Nacional de Prospecção de Metais do Grupo da Platina. Geologia e prospecção geoquímica/aluvionar da área Corumbiara/ Chupinguaia-Rondônia. Informe de Recursos Minerais. Serie Metais do Grupo da Platina e Associados, 6. CPRM, Porto Alegre (in Portuguese).

Sadowski, G.R., Bettencourt, J.S., 1996. Mesoproterozoic tectonic correlations between eastern Laurentia and western border of the Amazon Craton. Precambrian Research 76, 213–227.

Santos, J.O.S., Hartmann, L.A., Hartmann, L.A., Gaudette, H.E., Groves, D.I., McNaughton, N.J., Fletcher, I.R., 2000. A new understanding of the provinces of Amazon craton

based on integration of field mapping and U–Pb and Sm–Nd geochronology. Gondwana Research 3, 489–506.

Santos, J.O.S., Rizzotto, G., Easton, M.R., Potter, P.E., Hartmann, L.A., McNaughton, N.J., 2002. The Sunsás Orogen in Western Amazon Craton, South America and correlation with the Grenville Orogen of Laurentia, based on U–Pb isotopic study of detrital and igneous zircons. Geological Society of America, 2002 Denver Annual Meeting, Precambrian Geology, pp. 122–128.

Santos, J., Rizzotto, G.J., Potter, P., Mcnaughton, N., Matos, R., Hartmann, L., Chemale Jr., F., Quadros, M., 2008. Age and autochthonous evolution of the Sunsás Orogen in West Amazon Craton based on mapping and U Pb geochronology. Precambrian Research 165, 120–152.

Saunders, A.D., Norry, M.J., Tarney, J., 1991. Fluid influence on the trace element compositions of subduction zone magmas. Philosophical Transactions of the Royal Society of London 335, 377–392.

Schmidt, M.W., 1992. Amphibole composition in tonalites as a function of pressure: an experimental calibration of the Al-in-hornblende barometer. Contributions to Mineralogy and Petrology 110, 304–310.

Schobbenhaus, C., 2001. Geological map of south America, scale 1:5000000, CGMW-CPRM-DNPM-UNESCO, Brasilia, Brazil.

Shervais, J.W., 2001. Birth, death and resurrection: the life cycle of suprasubduction zone ophiolites. Geochemistry, Geophysics, Geosystems 2 (Paper 2000GC000080).

Stern, R.J., Bloomer, S.H., 1992. Subduction zone infancy: examples from the Eocene Izu–Bonin–Mariana and Jurassic California. Geological Society of America Bulletin 104, 1621–1636.

Sun, S.S., 1987. Chemical composition of Archaean komatiites: implications for early history of the Earth and mantle evolution. Journal of Volcanology and Geothermal Research 32, 67–82.

Sun, S.S., McDonough, W.E., 1989. Chemical and isotopic systematics of oceanic basalts: implications for mantle composition and processes. In: Saunders, A.D., Norry, M.J. (Eds.), Magmatism in the Ocean Basins: Geological Society London, Spec. Publ., 42, pp. 313–345.

Taylor, B., Martinez, F., 2003. Back-arc basin basalt systematics. Earth and Planetary Science Letters 210, 481–497.

Taylor, S.R., McLennan, S.M., 1985. The continental crust: its composition and evolution. Blackwell Scientific Publication, Oxford, p. 312.

Teixeira, W., Tassinari, C.C.G., 1984. Caracterização geocronológica da província Rondoniana e suas implicações geotectônicas. Simpósio Amazônico. Manaus, 2. SBG/DNPM, Atas, pp. 87–91 (in Portuguese).

Tohver, E., van der Pluijm, B.A., Van der Voo, R., Rizzotto, G., Scandolara, J.E., 2002. Paleogeography of the Amazon craton at 1.2 Ga: early Grenvillian collision with the Llano segment of Laurentia. Earth and Planetary Science Letters 199, 185–200.

Tohver, E., van der Pluijm, B., Mezger, K., Essene, E., Scandolara, J., Rizzotto, G., 2004a. Significance of the Nova Brasilândia metasedimentary belt in western Brazil: redifining the Mesoproterozoic boundary of the Amazon craton. Tectonics 23, TC6004.

Tohver, E., Bettencourt, J.S., Tosdal, R., Mezger, K., Leite, W.B., Payolla, B.L., 2004b. Terrane transfer during the Grenville orogeny: tracing the Amazonian ancestry of southern Appalachian basement through Pb and Nd isotopes. Earth and Planetary Science Letters 228, 161–176.

Tohver, E., Teixeira, W., van der Pluijm, B., Geraldes, M., Bettencourt, J.S., Rizzotto, G.J., 2006. Restored transect across the exhumed Grenville orogen of Laurentia and Amazonia, with implications for crustal architecture. Geology 34, 669–672.

Unrug, R., 1992. The supercontinent cycle and Gondwana assembly: component cratons and the timing of suturing events. Journal of Geodynamics 16, 215–246.

Vernon, R.H., 1970. Comparative grain-boundary studies in some basic and ultrabasic granulites, nodules and cumulates. Scottish Journal of Geology 6, 337–351.

Weil, A.B., Van der Voo, R., Niocaill, C.M., Meert, J.G., 1998. The Proterozoic supercontinent Rodinia: paleomagnetically derived reconstructions for 1100 to 800 Ma. Earth and Planetary Science Letters 154, 13–24.

Winchester, J.A., Floyd, P.A., 1977. Geochemical discrimination of different magma series and their differential products, using immobile elements. Chemical Geology 20, 325–344.

Wood, B.J., Banno, S., 1973. Garnet–orthopyroxene and orthopyroxene–clinopyroxene relationships in simple and complex systems. Contributions to Mineralogy and Petrology 4, 109–124.

Zhao, G.C., Cawood, P.A., Wilde, S.A., Sun, M., 2002. Review of global 2.1–1.8 Ga orogens: implications for a pre-Rodinia supercontinent. Earth Science Reviews 59, 125–162.

Zhao, G.C., Sun, M., Wilde, S.A., Li, S.Z., 2004. A Paleo-Mesoproterozoic supercontinent: assembly, growth and breakup. Earth Science Reviews 67, 9–123.

Zhao, G.C., Cao, L., Wilde, S.A., Sun, M., Choe, W.J., Li, S.Z., 2006. Implications based on the first SHRIMP U–Pb zircon dating on Precambrian granitoid rocks in North Korea. Earth and Planetary Science Letters 251, 365–379.